

This dissertation has been  
microfilmed exactly as received 70-6913

WHITE, Marvin Hart, 1937-  
CHARACTERIZATION OF MICROWAVE  
TRANSISTORS.

The Ohio State University, Ph.D., 1969  
Engineering, electrical

University Microfilms, Inc., Ann Arbor, Michigan

© Marvin Hart White 1970

ALL RIGHTS RESERVED

\ CHARACTERIZATION OF MICROWAVE TRANSISTORS

DISSERTATION

Presented in Partial Fulfillment of the Requirements for  
the Degree Doctor of Philosophy in the Graduate  
School of The Ohio State University

By

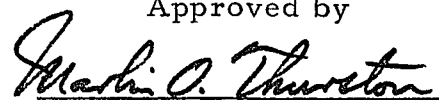
Marvin Hart White, A. S. , B. S. E. , M. S.

\* \* \* \* \*

The Ohio State University

1969

Approved by



Adviser

Department of Electrical  
Engineering

## ACKNOWLEDGMENTS

I should like to acknowledge the guidance and encouragement received from Professor Marlin O. Thurston through graduate studies, industrial work, and this dissertation. I wish to express my gratitude to Dr. Gene Strull, for his interest and encouragement, and to the scientists in the Solid-State Systems Technology Laboratory, Westinghouse Defense and Space Center, Baltimore, Maryland, for their technical assistance. My wife Sophia and son David deserve special mention for their family encouragement.

## VITA

- September 9, 1937 . . . . . Born - Bronx, New York
- 1957 . . . . . A. S., Henry Ford Community College, Dearborn, Michigan.
- 1960 . . . . . B. S. E., Physics and Mathematics, University of Michigan, Ann Arbor, Michigan.
- 1961 . . . . . M. S., Physics, University of Michigan, Ann Arbor, Michigan.
- 1961-1966 . . . . . Engineer, Solid-State Systems Technology Laboratory, Westinghouse Defense and Space Center, Baltimore, Maryland.
- 1966-1968 . . . . . Teaching Associate, Department of Electrical Engineering, The Ohio State University, Columbus, Ohio.
- 1968- . . . . . Senior Engineer, Solid-State Systems Technology Laboratory, Westinghouse Defense and Space Center, Baltimore, Maryland.

## PUBLICATIONS

More than ten publications in the area of solid-state devices. For example, M. H. White and J. R. Cricchi, "Complementary MOS Transistors", Solid-State Electronics, 9, pp. 991-1008, October 1966.

Contributed chapters to the following books:  
Semiconductors and Semimetals, Vol. 6, Semiconductor Applications, Chpt. "MOS Transistors", Marvin H. White, Academic Press, New York (1970).

VITA (Continued)

PUBLICATIONS (Continued)

Integrated Electronic Systems, Westinghouse Staff of Science and Technology, Prentice-Hall, New York (1970).

FIELDS OF STUDY

Major Field: Electrical Engineering

Studies in Solid-State Devices and Semiconductor Physics.  
Professor Marlin O. Thurston and Ibriham Adawi.

Studies in Control Systems.                      Professor Carlin F. Weimer

Studies in Applied Mathematics.              Professor Stefan Drobot

Studies in Quantum Chemistry.              Professor William J. Taylor

## TABLE OF CONTENTS

ACKNOWLEDGMENTS . . . . .	ii
VITA . . . . .	iii
LIST OF TABLES . . . . .	vii
LIST OF FIGURES . . . . .	viii
ABSTRACT . . . . .	1
Chapter	
I. INTRODUCTION . . . . .	5
1.1 Historical Review	
1.2 Scope of Thesis	
II. PHYSICS OF MICROWAVE TRANSISTOR OPERATION .	16
2.1 Introduction (Carrier Injection Level)	
2.2 Subsurface Sheet Resistance, $R_{ss}(0)$	
2.3 Modulation of the Subsurface Sheet Resistance, $R_{ss}(m)$	
2.4 Microwave Transistor Design Considerations	
2.5 Neutral and Space-Charge Capacitance	
2.6 Collector Junction Displacement	
III. MICROWAVE TRANSISTOR SMALL-SIGNAL EQUIVALENT CIRCUIT . . . . .	44
3.1 Introduction	
3.2 Base Charging Circuit Time Constant, $r'_b C_c$	
3.3 The T-Equivalent Circuit	
3.4 Current-Gain Bandwidth Product, $f_T$	
IV. SCATTERING PARAMETER FORMULATION . . . . .	55
4.1 Introduction to Scattering or S-Parameters	
4.2 S-Parameter Formulation in Terms of Device Parameters	
4.3 Maximum Unilateral Power Gain U(MAG) and $f_{MAX}$	
V. MICROWAVE TRANSISTOR DESIGN AND FABRICATION . . . . .	69

TABLE OF CONTENTS (Continued)

Chapter

VI.	EXPERIMENTAL RESULTS . . . . .	80
	6.1 Microwave Measurements	
	6.2 Device Test Structure	
	6.3 Transistor Equivalent Circuit Parameters	
VII.	CONCLUSIONS . . . . .	98
	BIBLIOGRAPHY . . . . .	101

## LIST OF TABLES

Table		Page
1.	Comparison of Microwave Transistor Designs for $x_E = 0.3$ micrometer and $x_C = 0.4$ micrometer . . . . .	35
2.	Comparison of Microwave Transistor Designs for $x_C - x_E = W = 0.1$ micrometer and $C_B = 3 \times$ $10^{15}$ atoms/cm <sup>3</sup> . . . . .	35
3.	Impurity Gradients in a Microwave Transistor $C_D = 8 \times 10^{20}$ ; $C_A = 2 \times 10^{19}$ $C_B = 3 \times 10^{15}$ . . . . .	39
4.	Effect of the built-in Electric Field in the Base Region Upon the $\omega_\alpha$ and $m$ of a Microwave Transistor. . . . .	51



## LIST OF ILLUSTRATIONS

Figure		Page
1	Evolution of High Frequency Transistor Technology . . .	7
2	Frequency Response of the Transistor . . . . .	11
3	Cross Section of a Microwave Transistor . . . . .	17
4	NPN Transistor Impurity Profile . . . . .	24
5	Variation of $R_{ss}$ with Base Width, $W$ . . . . .	26
6	Impurity Profile of a Microwave Transistor . . . . .	27
7	Effect of Background Concentration, $C_B$ , on the Time Constant $\tau = R_{ss} C_a$ . . . . .	33
8	Effect of the Junction Depth on the Time Constant, $\tau = R_{ss} C_a$ . . . . .	34
9	Neutral and Space-Charge Capacitances in a Linearly Graded P-N Junction Under Forward Bias . . . . .	37
10	Effect of Impurity Gradient on the Neutral and Space- Charge Capacitance in a Linearly Graded P-N Junction Under Forward Bias . . . . .	40
11	Displacement of the Space-Charge Region in a Linearly Graded Base-Collector P-N Junction With Increasing Current Density . . . . .	41
12	Cross-Section of a Double Base Strip, Single Emitter Strip Microwave Transistor, Base Charging Circuit Time Constant, $r_b' C_c$ , Equivalent Circuit . . . . .	45
13	Small-Signal Lumped T-Equivalent Circuit of the Microwave Transistor in the Common-Emitter Configuration . . . . .	49

## LIST OF ILLUSTRATIONS (Continued)

Figure		Page
14	Two-Port Microwave Transistor (S-Parameter Characterization) . . . . .	56
15	Small-Signal Equivalent Circuits of the Common-Emitter Microwave Transistor at Input and Output Ports . . . . .	60
16	S-Parameters versus Increasing Frequency for a Common-Emitter Microwave Transistor . . . . .	63
17	Transducer Power Gain, $G_T$ , and Unilateral Maximum Power Gain, $U(\text{MAG})$ Versus Frequency for a Common-Emitter Microwave Transistor . . . . .	66
18	Fabrication of a Silicon Microwave Transistor . . . . .	71
19	Photographic Masks, 487 Series, 1 through 5 (500 X) . . . . .	73
20	Silicon Microwave Transistor . . . . .	79
21	Microwave Transistor Test Fixture . . . . .	81
22	Microwave Transmission Line Geometry . . . . .	82
23	Electrical Circuit Diagram of RF and Biasing for the Microwave Transistor . . . . .	84
24	Block Diagram $S_{21}$ and $S_{12}$ (Measurement of Transmission Parameters) . . . . .	85
25	Block Diagram $S_{11}$ and $S_{22}$ (Measurement of Reflection Parameters) . . . . .	87
26	S-Parameters for an Experimental Silicon Microwave Transistor in the Frequency Range from 1.0 to 6.0 GHz ( $I_c = 10 \text{ mA}$ , $V_c = 10 \text{ V}$ ) . . . . .	88

LIST OF ILLUSTRATIONS (Continued)

Figure		Page
27	Transducer Power Gain, $G_T$ (lower curve) and Unilateral Power Gain, $U(\text{MAG})$ (upper curve) for a Silicon Microwave Transistor . . . . .	89
28	Device Test Structure to Determine Elements of the Base-Charging Circuit Time Constant, $r_b' C_c$ . . . . .	90

## ABSTRACT

### CHARACTERIZATION OF MICROWAVE TRANSISTORS

By

Marvin Hart White, Ph. D.

The Ohio State University, 1969

Professor Marlin O. Thurston, Advisor

In this thesis, the microwave transistor is characterized by a small-signal lumped T-equivalent circuit through which the small-signal scattering parameters, or s-parameters, are derived in terms of the physical device parameters. The s-parameters describe the transmission and reflection of power into and out of the microwave transistor. Measurements are carried out with the transistor embedded in a coaxial transmission line system of characteristic impedance  $Z_0$ . The behavior of these s-parameters versus frequency for a common-emitter stage is predicted and verified with experimental silicon bipolar microwave transistors. The design and fabrication of the silicon microwave transistors are described in detail in the thesis. The physical mechanisms that influence transistor performance are related to the physical device parameters. This work is, in the author's opinion, the first reported attempt to characterize, both

analytically and physically, the small-signal properties of the microwave transistor.

The lumped, small-signal, T-equivalent circuit for the microwave transistor provides an adequate model to explain the frequency variation of the s-parameters. The input and output of the microwave transistor may be characterized by a series RLC and parallel  $R_o C_o$  equivalent circuit, respectively. This was substantiated by s-parameter measurements in the frequency range from 1.0 to 6.0 GHz. The microwave transistor was mounted on a microstrip line configuration that consisted of a strip conductor parallel to a ground plane. Measurements were performed with a Hewlett-Packard 8410A Network Analyzer system.

The silicon microwave transistor was designed to maximize the transducer  $G_T$  and maximum unilateral U(MAG) power gains. A combination of a small-signal lumped T-equivalent circuit and computer-generated curves of subsurface sheet resistance,  $R_{ss}$ , was used in the design approach. Shallow impurity profiles ( $x_E = 2000 \text{ \AA}$ ,  $x_C = 3000 \text{ \AA}$ ) and narrow emitter strips ( $h = 1.5$  micrometers) provided typical  $f_T$  greater than 4 GHz and  $f_{MAX}$  greater than 6 GHz. The shallow diffusion profiles minimized the product of the subsurface sheet resistance,  $R_{ss}$ , and the base-collector capacitance/area,  $C_a$ , for a specified collector

resistivity (e.g., 1 to 3 ohm-cm). These diffusion profiles provided steep impurity gradients at the emitter and collector junctions. These gradients reduced the neutral capacitance of the emitter-base junction and base widening of the collector junction.

The fabrication of silicon microwave transistors required uniform thin photoresist to print the micrometer emitter strips. Low temperature emitter diffusions were required to minimize the base push-out or emitter-dip effect and to prevent a high incidence of emitter-collector shorts. A (100) orientation was selected for the silicon substrates to reduce the dislocation density and emitter-collector shorts. An emitter-dip etch was employed to avoid a difficult alignment of the contact metallization mask for the emitter strips. Finally, the molybdenum-gold metallization system was selected to replace the conventional aluminum contact metallization. The aluminum metallization resulted in a large number of emitter-base shorts, which was attributed to aluminum migration along the Si-SiO<sub>2</sub> interface at low temperatures.

As a result of the investigations performed for this thesis, it is concluded that the microwave performance of the transistor amplifier is limited by the base contact resistance and the emitter lead inductance. The development of techniques to minimize the contact

resistance, such as high surface concentration diffusions and surface preparation of the semiconductor, are important to increase the  $f_{MAX}$  of the transistor. The emitter lead inductance may be reduced by the use of beam-lead technology. It is anticipated that, through these developments, the Silicon microwave transistor will provide direct signal amplification in the X-band microwave region.

## CHAPTER I

### INTRODUCTION

#### 1.1 Historical Review

In December, 1947, Walter Brattain and John Bardeen of the Bell Telephone Laboratories built the first practical transistor, which was announced formally in July, 1948.<sup>1</sup> Their device was a point-contact structure that used two metal "cat's whiskers" in contact with a polycrystalline slab of germanium. This electronic device, which was eventually to replace the vacuum tube in electronic communication systems, was the culmination of studies and experiments that had lasted for almost ten years. Their group leader, William Shockley, predicted, in 1949, that the point-contact transistor would be replaced by the junction transistor.<sup>2</sup> This device was demonstrated as early as 1951.<sup>3</sup> (In 1956, the trio of Bardeen, Brattain, and Shockley was awarded the Nobel Prize for its achievements.) In the two decades

---

<sup>1</sup>J. Bardeen and W. Brattain, Phys. Rev., 74, 230 (1948).

<sup>2</sup>W. Shockley, Bell Syst. Tech. J., 28, 435 (1949).

<sup>3</sup>W. Shockley, M. Sparks, and G. K. Teal, Phys. Rev., 83, 151 (1951).



following the announcement of the transistor, there were many contributions to the growth of the high frequency transistor technology.

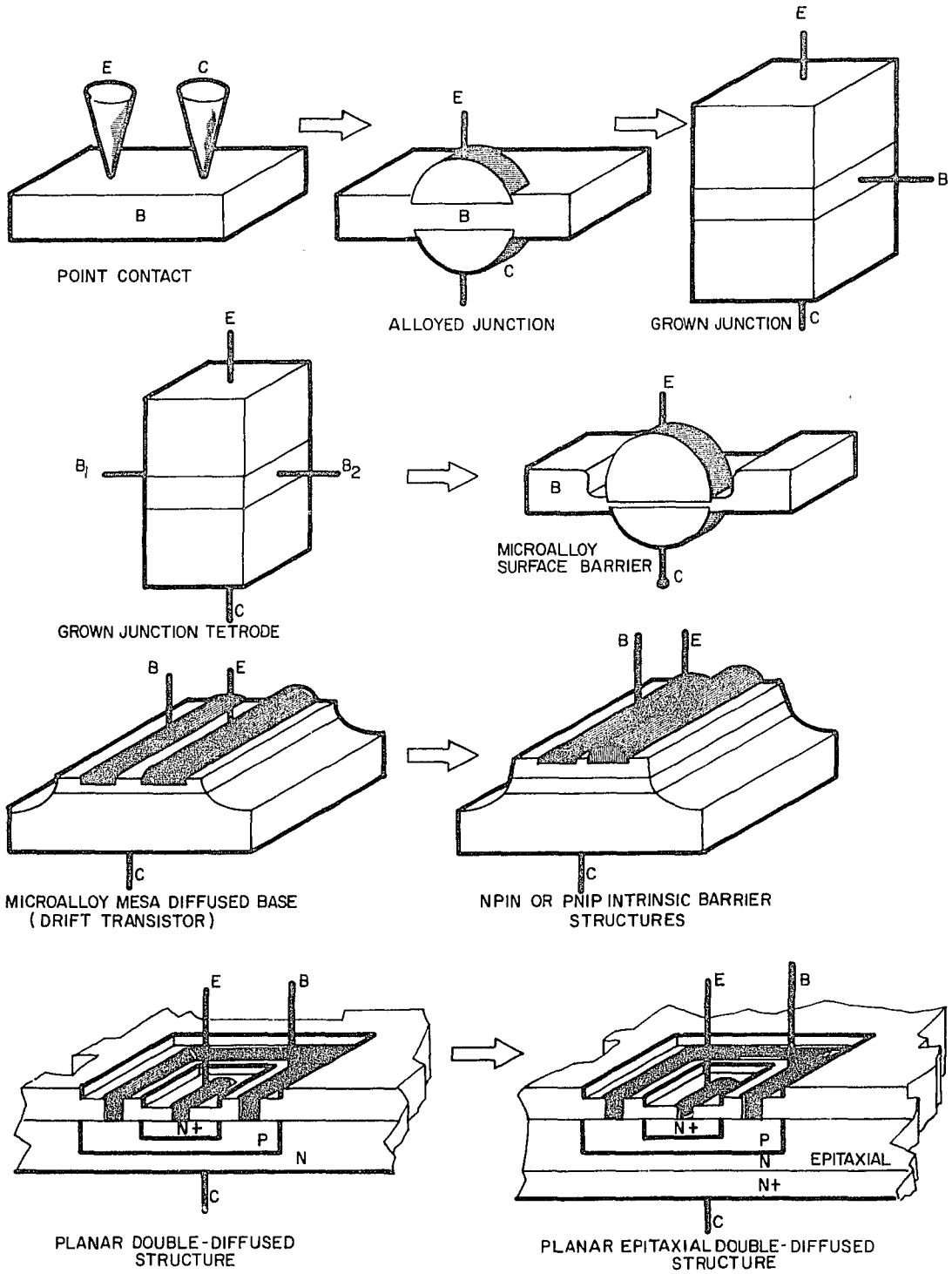
Figure 1 illustrates the cross-sectional views of the principal high frequency transistor structures that were fabricated during this period.

In the point-contact transistor<sup>1</sup>, the boundary-layer of a reverse-biased point-contact collector was the current path, which was controlled by a forward-biased point-contact emitter. The operation of this device was largely dependent upon the surface treatments and metal-semiconductor forming processes. The next significant transistor structure was the alloy-junction device<sup>4, 5</sup>, in which dots of impurity elements were alloyed on either side of a germanium or silicon wafer. These transistors, because of their large base widths, were limited to the audio frequency range. Another technique of transistor fabrication was the grown junction device, in which impurity layers were developed, while the semiconductor crystal was withdrawn from the melt.<sup>3</sup> The transistors were then cut from the crystal in a direction parallel to the axis, so that each transistor spanned the impurity layer. Through careful control of the crystal pulling, it was possible to obtain thin base widths with transistor amplification in the megahertz

---

<sup>4</sup>R. R. Law, et. al., Proc. IRE, 40, 1352 (1952).

<sup>5</sup>J. S. Saby, Proc. IRE, 40, 1358 (1952).



S9446A-VB-1

Figure 1. Evolution of High Frequency Transistor Technology

region. A modification of this grown junction device was the junction tetrode<sup>6</sup>, in which an appropriately biased second base electrode restricted the current path. These devices were characterized by low transverse base resistance and demonstrated signal amplification in the low VHF range (30 to 300 MHz).

The microalloy surface-barrier transistor<sup>7, 8</sup> was the next significant fabrication technique in the development of high frequency transistors. The electro-chemical "jet etching" of thin base regions provided signal amplification in the VHF band. The microalloy technique was further extended to realize the alloyed emitter, diffused-base, mesa drift-field transistor<sup>9, 10</sup>, which provided oscillators throughout the VHF band. A modification of the diffused-base transistor was the intrinsic-barrier transistor<sup>11</sup>, which had an additional high resistivity (intrinsic) region adjacent to the collector to reduce the collector capacitance. These NPIN and PNIP structures were capable of signal

---

<sup>6</sup>R. L. Wallace, et. al., Proc. IRE, 40, 1395 (1952).

<sup>7</sup>W. E. Bradley, Proc. IRE, 41, 1702 (1953).

<sup>8</sup>A. D. Rittmann, et. al., IRE Trans. on Electron Devices, ED-5, 49 (1958).

<sup>9</sup>H. Kroemer, Arch. Elekt. Übertragung, 8, 223; 363; 449 (1954).

<sup>10</sup>C. A. Lee, Bell Syst. Tech. J., 35, 23 (1956).

<sup>11</sup>J. M. Early, Bell Syst. Tech. J., 33, 517 (1954).

amplification through the VHF band and oscillations in the low UHF range (300 to 3000 MHz).

In 1960, the planar process, which employed oxide-masking and diffusion technologies, was introduced to the scientific and engineering community.<sup>12</sup> The resultant planar double-diffused silicon transistors provided signal amplification in the low UHF range and oscillations in the microwave region (L-band; 1000 to 2000 MHz; 1 to 2 GHz). In 1962, the development of a silicon epitaxial growth process<sup>13</sup> reduced the collector series resistance, which extended the frequency response of the transistors. By the late 1960's, microwave transistors had been fabricated that were capable of amplification in the C-band (4.0 to 7.0 GHz) and oscillation in the low X-band range (7.0 to 12.4 GHz). In a period of two decades, transistor base width had been decreased from several mils to a few thousand angstroms through the close control of shallow diffusions.<sup>14</sup> In addition, the width of the emitter strip had

---

<sup>12</sup>J. A. Hoerni, IRE Trans. on Electron Devices, ED-8, 178 (1961). This work was originally presented at the fall meeting of the International Electron Device Conference in October, 1960, Washington, D. C.

<sup>13</sup>Many workers were responsible for the improvements in silicon epitaxial growth technology. See, for example, J. Sigler and S. B. Watelski, Solid State J., 2, 33 (1961).

<sup>14</sup>Many workers are responsible for the improvements in diffusion technology. A recent report is, R. M. McLouski, NASA Contractor Report, NASA CR-597 (1966).

decreased from several mils to a few micrometers by improved photolithographic technology.<sup>15</sup> The overall result of these process improvements has been an increase in the current-gain bandwidth product,  $f_T$ , and the maximum frequency of oscillation,  $f_{MAX}$ , as shown in Figure 2.

As the frequency response of the transistor increased during the two decades illustrated in Figure 2, the small-signal equivalent circuit representation of the transistor had to be altered. The first model of the transistor was the T-equivalent circuit, which was developed for the point-contact transistor.<sup>16</sup> The three elements of the T-equivalent circuit, excluding the current gain, were essentially independent of frequency, up to several megahertz, for the point-contact transistor; however, this was not the case for the junction transistor. The T-equivalent circuit was modified for the junction transistor by including the effects of base resistance through base-width modulation<sup>17</sup> and the collector capacitance,  $C_c$ .<sup>18</sup> The frequency variation of the common-base short-circuit current gain,  $\alpha(\omega)$ , was introduced through an

<sup>15</sup> Many workers are responsible for the improvements in photolithographic technology. A recent report is, C. J. Taylor, NASA Contractor Report, NASA CR-597 (1966).

<sup>16</sup> R. M. Ryder and R. J. Kircher, Bell Syst. Tech. J., 28, 370 (1949).

<sup>17</sup> J. M. Early, Proc. IRE, 40, 1401 (1952).

<sup>18</sup> J. M. Early, Bell Syst. Tech. J., 32, 1271 (1953).

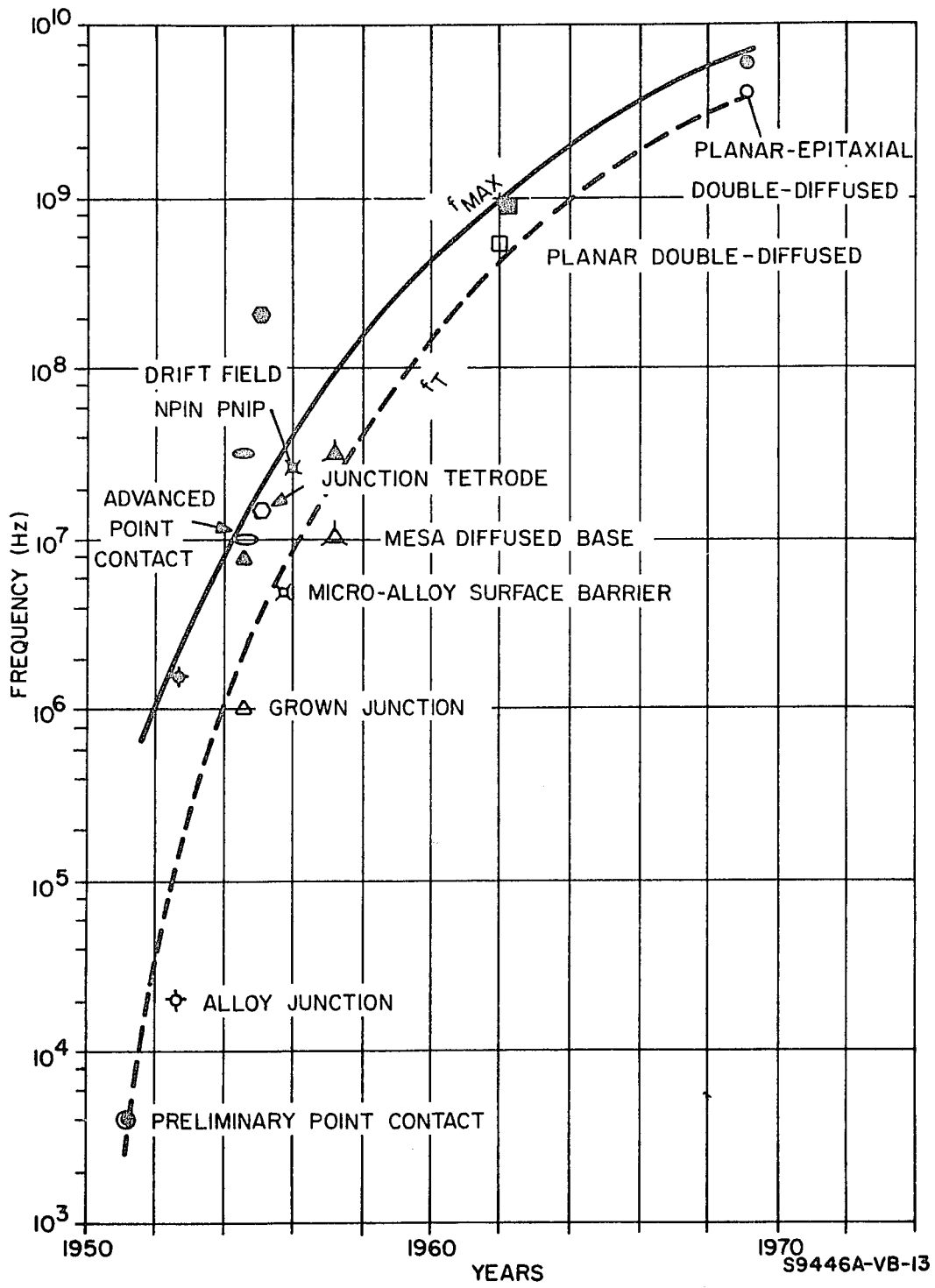


Figure 2. Frequency Response of the Transistor

equivalent single-pole function<sup>19</sup> that defined the so-called "alpha cut-off frequency",  $\omega_\alpha$ . The principal disadvantage of the T-equivalent circuit was the inherent feedback represented by the common element between input and output ports. Thus, the conventional T-equivalent circuit was modified to the hybrid- $\pi$  model<sup>20</sup>, which neglected the internal feedback in the common-emitter stage and attributed the entire feedback of the amplifier to the collector-base capacitance.

With the advent of the diffused-base transistor and its high internal electric fields, the carrier transit times in the base region were significantly reduced; however, the phase characteristics of the current gain,  $\alpha(\omega)$ , were altered by these electric fields. The variation of current gain and phase with frequency was described with a single-pole network that incorporated a linear excess phase shift.<sup>21</sup> The T-equivalent circuit was appropriately modified to take into account the electric field in the base region, depletion-layer capacitance of the emitter-base junction and series resistances in the emitter and collector legs of the equivalent circuit.<sup>22</sup> This analysis was performed with

---

<sup>19</sup>R. L. Pritchard, Proc. IRE, 40, 1476 (1952).

<sup>20</sup>L. J. Giacoletto, RCA Review, 15, 506 (1954).

<sup>21</sup>D. E. Thomas and J. E. Moll, Proc. IRE, 46, 1177 (1958).

<sup>22</sup>R. P. Abraham, IRE Trans. on Electron Devices, ED-7, 59 (1960).

the h-parameter representation for the VHF-UHF frequency range. The hybrid- $\pi$  has also been employed<sup>23, 24</sup> to describe the UHF transistor with the use of the y-parameter representation.

## 1.2 Scope of Thesis

Although microwave and UHF transistors have been available commercially for almost a decade, there has been little attempt to characterize these devices in terms of their small-signal properties. One of the principal problems, until recently, has been the difficulty in carrying out the measurements. Formerly, the y-(admittance) parameters were employed to describe the VHF-UHF performance of transistors; however, the necessary short-circuit conditions for these parameters were difficult to realize. In addition to the problem of terminations, the transistor would frequently break into oscillations under the short-circuit terminations because of conditional stability and render any measurements impossible. With y- and h-parameter characterization, it was extremely difficult to characterize the microwave and UHF transistors accurately. A method of circumventing this

---

<sup>23</sup>G. Johnson, Solid-State Communications, Chpt. 4, Ed. by J.R. Miller (New York: McGraw-Hill, 1966).

<sup>24</sup>Westinghouse Staff of Science and Technology, Integrated Electronic Systems, Chpt. 6, (New York: Prentice-Hall, 1970).



problem has been the use of scattering, or s-parameters.<sup>25</sup> These s-parameters describe the transmission and reflection of power into and out of a microwave network such as a transistor. The measurements are carried out with the transistor embedded in a coaxial transmission line system of characteristic impedance  $Z_0$ . An important advantage of the s-parameter characterization derives from the fact that traveling waves, in contrast with terminal voltages and currents, do not vary in magnitude at various points along a lossless transmission line. This enables the s-parameters to be measured at distances far-removed from the terminals of the microwave transistor.<sup>26, 27</sup>

In this thesis, the small-signal T-equivalent circuit of the transistor is modified through the inclusion of emitter and base lead inductances, series and contact resistances in the emitter and collector legs of the circuit, and parasitic capacitances to characterize the small-signal properties of the microwave transistor. The base-charging circuit time constant,  $r_b' C_c$ , is analyzed with respect to the geometry of

---

<sup>25</sup>K. Kurokawa, IEEE Trans. on Microwave Theory and Techniques, MTT-13, 194 (1965).

<sup>26</sup>Y. Satoda and G. E. Bodway, IEEE J. of Solid-State Circuits, SC-3, 250 (1968).

<sup>27</sup>R. W. Anderson, Hewlett Packard J., 18, 13 (1967).

the microwave transistor (Chapter III). The s-parameters are derived from the modified T-equivalent circuit to relate the device parameters to the microwave performance of the transistor. The behavior of these s-parameters versus frequency for a common-emitter stage is predicted (Chapter IV) and verified with experimental silicon bipolar microwave transistors (Chapter VI). The design and fabrication of the experimental microwave transistors (Chapter V) and the s-parameter measurement techniques (Chapter VI) are described in detail. The physical mechanisms that influence the microwave transistor performance are discussed in Chapter II. This work is, in the author's opinion, the first reported attempt to characterize, both analytically and physically, the small-signal properties of the microwave transistor.

## CHAPTER II

### PHYSICS OF MICROWAVE TRANSISTOR OPERATION

#### 2.1 Introduction (Carrier Injection Level)

The level of carrier injection influences the performance of the microwave transistor. In practice, the microwave transistor is biased at a current density that maximizes the transducer power gain (refer to Chapter IV). The current density is typically greater than  $10^3$  A/cm<sup>2</sup>, which results in conductivity modulation of the base and collector regions, base-width widening, and an increase in neutral capacitance. In this section, the npn silicon transistor is discussed with respect to carrier injection level. Figure 3 illustrates a cross-sectional view of a microwave transistor. The electron current density in the longitudinal direction may be written as,

$$J_{nx} = q\mu_n n \xi_x + q D_n \frac{\partial n}{\partial x}. \quad (2-1)$$

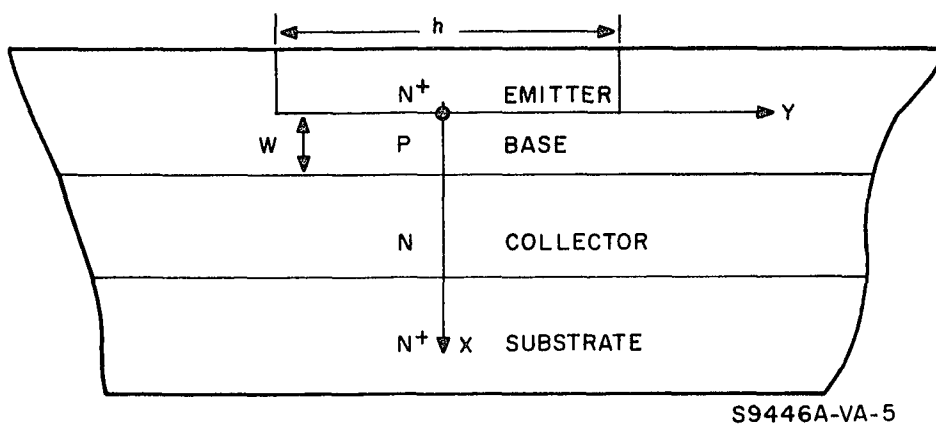


Figure 3. Cross Section of a Microwave Transistor

Since a reverse-biased p-n junction (i. e., the base-collector junction) blocks majority carriers, the electric field<sup>1</sup> is determined from the condition

$$J_{px} = q \mu_p p \xi_x - q D_p \frac{\partial p}{\partial x} \stackrel{!}{=} 0$$

$$\xi_x = \frac{k_B T}{q} \frac{1}{p} \frac{\partial p}{\partial x} \quad (2-2)$$

Substitution of equation 2-2 into 2-1 yields

$$J_{nx} = \frac{q D_n}{p} \frac{\partial(np)}{\partial x} \quad (2-3)$$

The transverse electron current is small with respect to the longitudinal electron current (i. e.,  $J_{ny} \ll J_{nx}$ ) and the latter may be considered as constant over the base region. With this assumption, equation 2-3 becomes,

$$J_{nx} = \frac{q D_n n(0) p(0)}{\int_0^W p dx} \quad (2-4)$$

with the boundary condition<sup>2</sup>  $n(W) = 0$ . The charge neutrality condition is

$$p = N_A + n. \quad (2-5)$$

---

<sup>1</sup> an exponential variation of impurity density in the base region leads to a constant electric field as seen in equation (2-2).

<sup>2</sup> The actual boundary condition is  $n(W) = J_n / q V_L$ ; where,  $V_L$  is the maximum scatter-limited velocity of carriers.

Thus, the integral of the hole density across the base region becomes

$$\int_0^W p \, dx = \int_0^W N_A \, dx + \int_0^W n \, dx. \quad (2-6)$$

If the electron current density,  $J_{nx}$ , and electric field,  $\xi_x$ , of equation 2-1 are considered to be constant over the base width, the electron density may be determined by integration of equation 2-1 with the boundary condition  $n(W) = 0$ .

$$n(x) = n(0) \left[ \frac{1 - e^{-2\eta(1-x/W)}}{2\eta} \right] \quad (2-7)$$

where,  $n(0) = J_{nx} W / q D_n$  is the injected carrier density at  $x = 0$  (i. e., the edge of the emitter-base depletion layer), and  $\eta = -q \xi_x W / 2k_B T$  is the electric field parameter. If  $\eta = 0$  (i. e., no internal electric field), the injected electron density becomes

$$n(x) = n(0) \left[ 1 - \frac{x}{W} \right] \quad (2-8)$$

which represents a linear variation of carrier density in the base region. Integration of equation 2-7 across the base region yields,

$$\int_0^W n(x) \, dx = \frac{n(0) W}{2} f(\eta) \quad (2-9)$$

where,  $f(\eta)$  is

$$f(\eta) = \frac{2 \left[ 2\eta - 1 + e^{-2\eta} \right]}{(2\eta)^2} \quad (2-10)$$

The electric field parameter is discussed in Chapter III with respect to the electrical equivalent circuit and the impurity profile in the base region. Combining equations 2-4, 2-6, and 2-9 yields,

$$J_{nx} = \frac{q D_n n(0)}{W} \frac{\left[ n(0) + N_A(0) \right]}{\left[ \bar{N}_A + \frac{n(0) f(\eta)}{2} \right]} \quad (2-11)$$

where,  $\bar{N}_A$  is the average acceptor concentration in the base region.

Defining

$$\bar{N}_A = k N_A(0) \quad (2-12)$$

enables us to write equation 2-11 in the form

$$J_{nx} = \frac{2 q D_n N_A(0)}{W} \frac{m_o (m_o + 1)}{(m_o f(\eta) + 2k)} \quad (2-13)$$

where,

$$m_o = \frac{n(0)}{N_A(0)} \quad (2-14)$$

is the modulation level at the edge of the base-emitter depletion layer.

For  $m_o \ll 1$  (low-level injection), the current density becomes

$$J_{nx} = \frac{q D_n n(0)}{W k} \quad (\text{low-level injection}) \quad (2-15)$$

while for  $m_o \gg 1$  (high-level injection), the current density is

$$J_{nx} = \frac{q 2 D_n n(0)}{W} \quad (\text{high-level injection}) \quad (2-16)$$

where the diffusion constant is doubled over the case of a uniform base region ( $k = 1$ ) at low-level injection.<sup>3</sup> For the double-diffused silicon microwave transistors discussed in these chapters, the value of  $k$  lies in the range from  $1/3$  to  $1/2$ . Thus, there is an improvement in the effective diffusion constant for double-diffused structures over the ideal uniform base transistor.

## 2.2 Subsurface Sheet Resistance, $R_{ss}(0)$

The subsurface sheet resistance has been briefly discussed in paragraph 2.1 with regard to the effect of modulation by injected minority carriers. In this paragraph, the subsurface sheet resistance,  $R_{ss}(0)$ , will be determined for typical microwave transistor impurity profiles through numerical calculations on the computer. The total mobility for uncompensated material may be written in the form

$$\frac{1}{\mu_p^i(x)} = \frac{1}{\mu_L} + \frac{1}{\mu_I^i(x)} \quad (2-17)$$

where,  $\mu_L$  is the lattice-scattered limited mobility, and  $\mu_I^i(x)$  is the uncompensated impurity-scattered limited mobility. The values of  $\mu_I^i(x)$  as a function of the impurity concentration are obtained by

---

<sup>3</sup>This is referred to as the Webster Effect from W. Webster, Proc. IRE, 41, 914 (1954). At high injection levels, the electric field is effectively washed-out.



subtraction of the value of  $\mu_L$ <sup>4</sup> from the published values of  $\mu_p'$ (x).<sup>5</sup>

The impurity-scattered limited mobility for compensated material (e. g., the base region of the microwave transistor) is determined by the expression<sup>6</sup>

$$\mu_I(x) = \left| \frac{C_A(x) - C_D(x) - C_B}{C_A(x) + C_D(x) + C_B} \right| \mu_I'(x) \quad (2-18)$$

where,  $C_A(x)$ ,  $C_D(x)$ , and  $C_B$  are the base, emitter, and collector concentrations, respectively. The total mobility for compensated material is obtained through the expression

$$\frac{1}{\mu_p(x)} = \frac{1}{\mu_L} + \frac{1}{\mu_I(x)}. \quad (2-19)$$

The subsurface sheet resistance at any depth, x, from the emitter may be formulated as follows:

$$G_{ss} = \frac{1}{R_{ss}} = \int_{x_j}^x q \mu_p(x) N_A(x) dx \quad (2-20)$$

where

$$N_A(x) = C_A(x) - C_D(x) - C_B. \quad (2-21)$$

---

<sup>4</sup>N. B. Hannay, Ed., Semiconductors, (New York: Rheinhold Publishing Corp., 1960).

<sup>5</sup>J. C. Irvin, Bell Syst. Tech. J., 41, 391 (1962).

<sup>6</sup>W. R. Runyan, Silicon Semiconductor Technology, (New York: McGraw-Hill, 1965).

Equation 2-20 may be written as a summation and integration in the manner

$$\frac{1}{R_{ss}} = q \sum_{N=1}^{M = \frac{x - x_j}{\Delta x}} \mu_p \left[ x_j + \frac{\Delta x}{2} + (N-1)\Delta x \right] \int_{x_j + (N-1)\Delta x}^{x_j + N\Delta x} N_A(x) dx \quad (2-22)$$

in which the mobility is considered constant in the center of a region  $\Delta x$ . In the analysis to follow, the subsurface sheet resistance is obtained for ideal Gaussian base and emitter diffusions into a constant background concentration, as shown in Figure 4. Thus, the net impurity concentration may be written as

$$N_A(x) = C_A e^{-x^2/L_A^2} - C_D e^{-x^2/L_D^2} - C_B \quad (2-23)$$

where,  $L_A$  and  $L_D$  are the characteristic diffusion lengths determined by the boundary conditions

$$N_A(x_E) = N_A(x_C) = 0. \quad (2-24)$$

$L_A$  and  $L_D$  are determined through an iterative solution of equations 2-23 and 2-24, with the initial value determined by neglecting  $C_B$ .<sup>7</sup>

---

<sup>7</sup>R. P. O'Grady, Microelectronics and Reliability, 7, 233 (1968). This technique is employed for base widths greater than 0.5 micrometers; however, for the small base widths of microwave transistors, an iterative solution was required to find  $L_A$  and  $L_D$ .

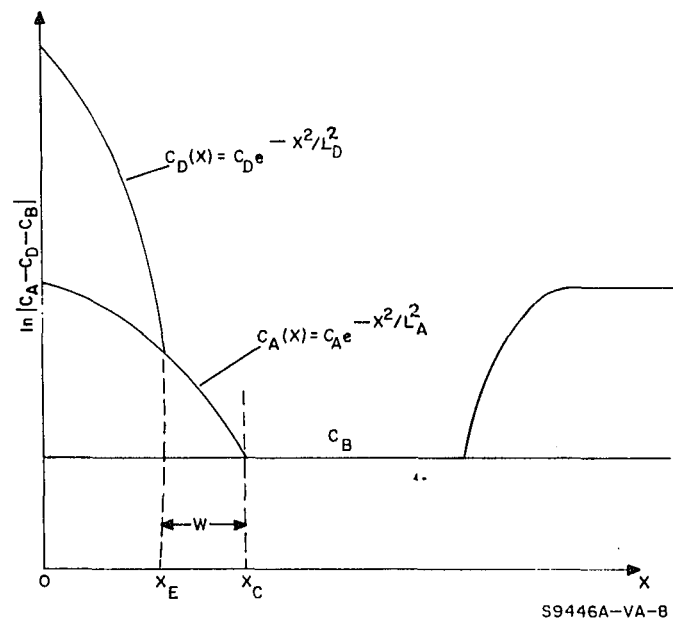


Figure 4. NPN Transistor Impurity Profile

Substitution of equation 2-23 into equation 2-22 and integrating from  $x_E$  to  $x_C$  (i. e., in equation 2-22  $x \rightarrow x_C$  and  $x_j \rightarrow x_E$ ), the  $R_{ss}$  is obtained. In practice,  $C_A$ ,  $C_D$ ,  $C_B$ ,  $x_E$ , and  $x_C$  are specified; and the hole mobility,  $\mu_p(x)$ , in the base region, free carrier concentration,  $p(x)$ , in the base region, and subsurface sheet resistance,  $R_{ss}$ , are determined by numerical calculations on the computer. A particular quantity of interest is the variation in  $R_{ss}$  with base width for a fixed collector junction depth. Figure 5 illustrates the numerical calculations performed for  $R_{ss}$  versus base width,  $W$ , under assumed junction depths and surface concentrations. Figure 6 illustrates the impurity profile of a microwave transistor with  $x_E = 0.2$  micrometers,  $x_C = 0.3$  micrometers,  $C_D = 8 \times 10^{20}$  atoms/cm<sup>3</sup>,  $C_A = 2 \times 10^{19}$  atoms/cm<sup>3</sup> and  $C_B = 3 \times 10^{15}$  atoms/cm<sup>3</sup>.

### 2.3 Modulation of the Subsurface Sheet Resistance, $R_{ss}$ ( $m_o$ )

The transverse electric field, which is developed by the flow of majority carrier base current, may be related to the longitudinal field through Kirchoff's Law (Maxwell's Equation) in the form

$$\nabla_{\mathbf{x}} \vec{\xi} = 0,$$

which becomes in 2-dimensions

$$\frac{\partial \xi_x}{\partial y} = \frac{\partial \xi_y}{\partial x} \quad (2-25)$$

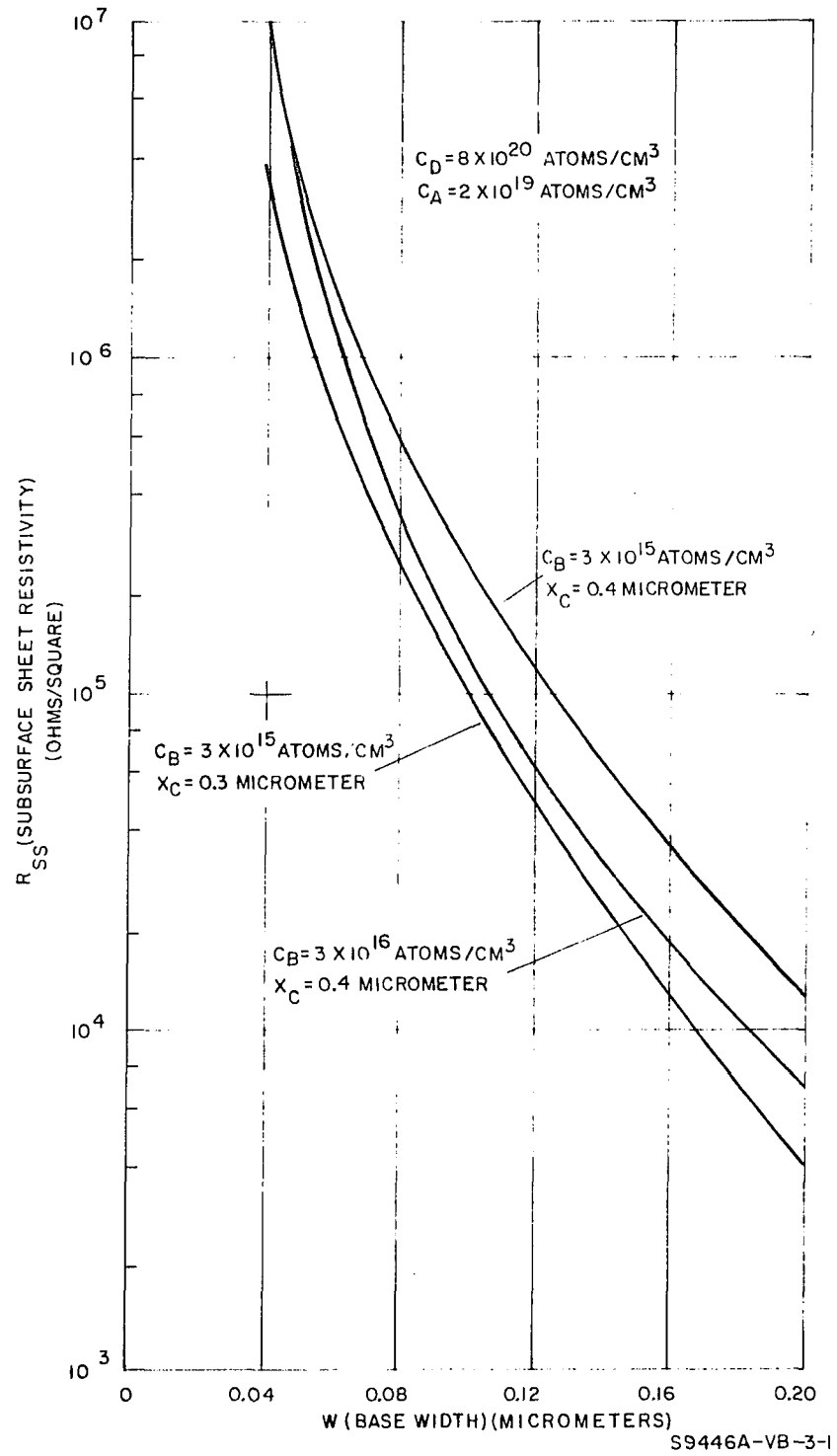


Figure 5. Variation of  $R_{SS}$  with Base Width,  $W$

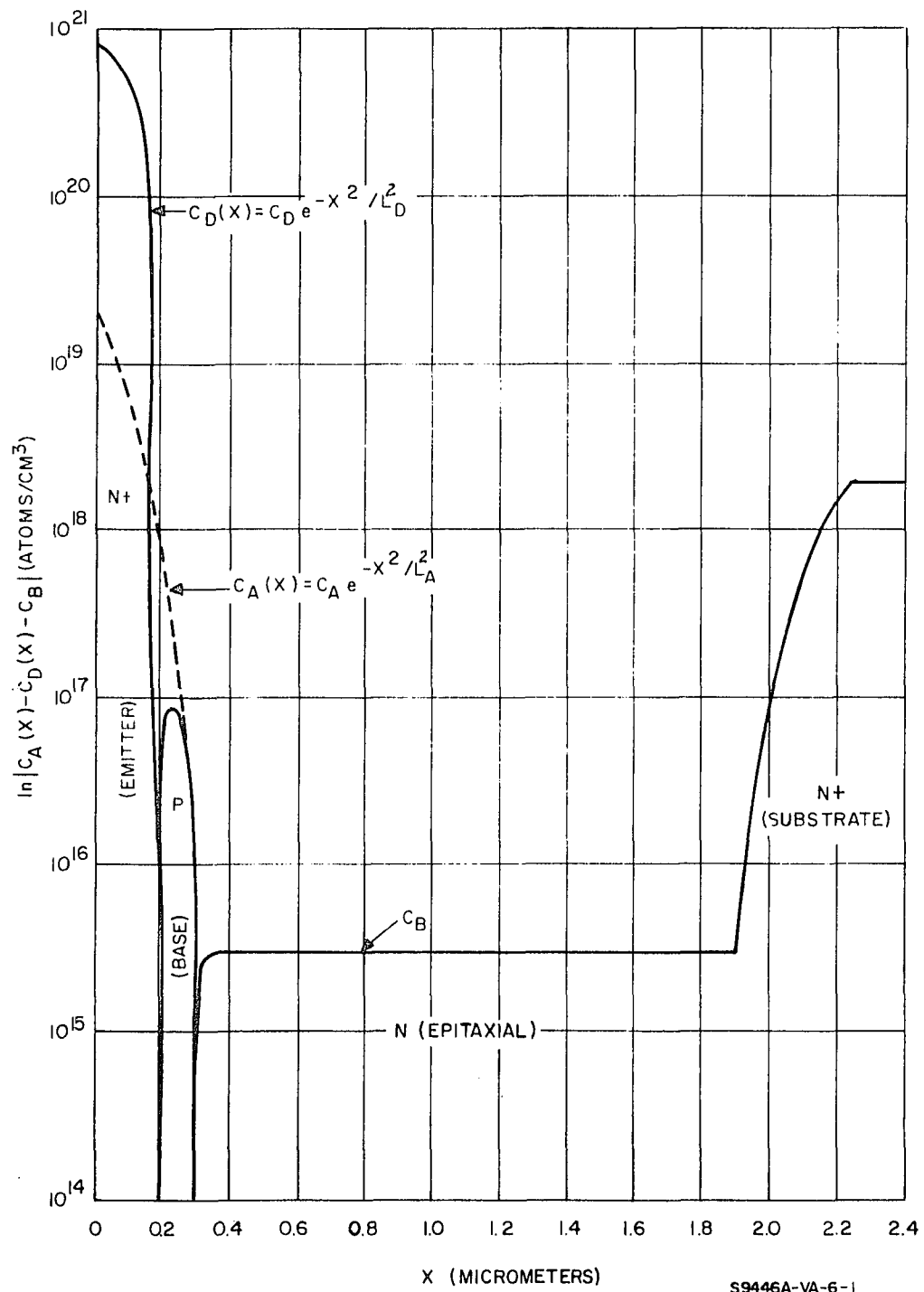


Figure 6. Impurity Profile of a Microwave Transistor

Combining equations 2-2 and 2-25, the transverse electric field becomes

$$\xi_y = \frac{k_B T}{q} \frac{1}{p} \frac{\partial p}{\partial y} + g(y) \quad (2-26)$$

where,  $g(y)$  is an arbitrary function of  $y$ . The transverse hole current density may be expressed as

$$J_{py} = q \mu_p p \xi_y - q D_p \frac{\partial p}{\partial y} = q \mu_p p g(y) \quad (2-27)$$

with the use of equation 2-26. Then,  $g(y)$  may be evaluated through the boundary condition<sup>8</sup>

$$n(0) p(0) = n_i^2 e^{qV(0)/k_B T} \quad (2-28)$$

which is the diode injection law. Differentiation of equation 2-28 yields

$$\frac{\partial}{\partial y} [n(0) p(0)] = -n(0) p(0) \frac{q}{k_B T} \xi_y(0). \quad (2-29)$$

From equation 2-5

$$\frac{\partial p(0)}{\partial y} = \frac{\partial n(0)}{\partial y} \quad (2-30)$$

which follows from the fact that  $N_A = N_A(x)$ . Equation 2-29 may be combined with equation 2-30 to yield

$$\frac{\partial p(0)}{\partial y} = \frac{-n(0) p(0)}{n(0) + p(0)} \frac{q}{k_B T} \xi_y(0). \quad (2-31)$$

---

<sup>8</sup> the symbol  $n(0)$  means  $n(x, y)_{x=0} = n(0, y)$ . Similarly,  $\xi_y(0)$  means  $\xi_y(x, y)_{x=0}$ . Equation 2-28 is strictly true only at low-level injection. At high injection levels, the gradient in the electro-chemical potentials in the space-charge region must be considered as pointed out by A. Nussbaum, Solid-State Electronics, 12, 177 (1969).

Combining equations 2-26 and 2-31 at  $x = 0$ , permits the evaluation of

$g(y)$

$$g(y) = \frac{[2n(0) + p(0)]}{[n(0) + p(0)]} \xi_y(0) \quad (2-32)$$

Substitution of equation 2-32 into 2-27 yields

$$J_{py} = q \mu_p p \frac{[2n(0) + p(0)]}{[n(0) + p(0)]} \xi_y(0) \quad (2-33)$$

which may be averaged over the base region

$$\overline{J_{py}} = \frac{1}{W} \int_0^W q \mu_p p dx \frac{[2n(0) + p(0)]}{[n(0) + p(0)]} \xi_y(0). \quad (2-34)$$

Combining equations 2-5, 2-14, and 2-34 yields

$$\overline{J_{py}} = \frac{\xi_y(0) (3m_o + 1)}{W (2m_o + 1)} \left[ \frac{1}{R_{ss}(0)} + \int_0^W q \mu_p n dx \right] \quad (2-35)$$

where,  $R_{ss}(0) = 1/q \int_0^W \mu_p N_A(x) dx$  is the subsurface sheet resistance at zero modulation level (i. e.,  $m_o = 0$ ). From equation 2-35, the subsurface sheet resistance under modulation may be written as<sup>9</sup>

$$R_{ss}(m_o) = \frac{(2m_o + 1) R_{ss}(0)}{(3m_o + 1) \left[ 1 + R_{ss}(0) \int_0^W q \mu_p n(x) dx \right]} \quad (2-36)$$

---

<sup>9</sup>V. A. Dhaka, IBM J. Res. and Dev., 12, 476 (1968) shows that  $R_{ss}(m) = \frac{2(m+1) R_{ss}(0)}{(m+2)(2m+1)}$  where  $m = n(0)/\overline{N}_A$  is defined in terms of the average base concentration. His results indicate slightly more conductivity modulation than the present analysis.



As an example, consider the injected carrier density of equation 2-7 and the impurity profile shown in Figure 6. Employing the mobility variation with distance shown in Figure 8, the modulated subsurface sheet resistance may be calculated for a specified injection level. For a value of  $m_o = 0.1$ , calculations yield  $R_{ss}(0.1) = 0.83 R_{ss}(0)$ , where  $R_{ss}(0) = 107,000$  ohms/square. For a value of  $m_o = 0.5$ , similar calculations show  $R_{ss}(0.5) = 0.49 R_{ss}(0)$ , which indicates that the subsurface sheet resistance may be reduced considerably at increased current densities.

#### 2.4 Microwave Transistor Design Considerations

The maximum frequency of oscillation,  $f_{MAX}$ , for a microwave transistor is a measure of the power gain (see paragraph 4.3). It may be expressed in the simple form

$$f_{MAX} = \sqrt{\frac{\alpha_o f_T}{8 \pi r_b' C_c}} \quad (2-37)$$

for the limiting situation of negligible parasitics and high current levels. The current-gain bandwidth product may likewise be written in the approximate form

$$f_T = \frac{1 + \alpha_o m}{2 \pi \alpha_o \omega_\alpha} = \frac{\lambda \bar{D}_n}{W^2} \quad (2-38)$$

where  $\lambda$  is determined from Table 4, in paragraph 3.3. For example,  $\lambda = 2$  when the electric field is zero in the base region of the transistor.

$\bar{D}_n$  is the average diffusion constant for minority carriers (electrons) and  $W$  is the electrical base width. Equation 2-38 represents an approximation to establish a design approach. In practice, all of the terms in equation (3-9) of paragraph 3.4 influence the  $f_T$ . The base-charging circuit time constant may be approximated (see paragraph 3.2) by the expression

$$r'_b C_c \doteq r'_{bb} C_i \quad (2-39)$$

where,  $r'_{bb}$  is the transverse base resistance beneath the emitter strip, and  $C_i$  is the capacitance of the base-collector junction beneath the emitter strip. Equation 2-39 may be written in terms of the subsurface sheet resistance  $R_{ss}$  and capacitance per unit area  $C_a$  in the manner,

$$r'_{bb} C_i = \frac{(R_{ss} h) (C_a h \ell)}{12 \ell} = \frac{R_{ss} C_a h^2}{12} \quad (2-40)$$

where,  $h$  is the emitter strip width and the factor of 12 accounts for the linear fall-off in base current.<sup>10</sup> Substitution of equations 2-38 and 2-40 into 2-37 yields

$$f_{MAX} = \frac{1}{2 \pi h W} \sqrt{\frac{3 \lambda \bar{D}_n}{R_{ss} C_a}} \quad (2-41)$$

---

<sup>10</sup>V. Uzunoglu, Semiconductor Network Analysis and Design, (New York: McGraw-Hill, 1964).

Equation 2-41 indicates the importance of narrow emitter strips and base widths for high  $f_{MAX}$ . Figure 7 illustrates the comparison of two impurity profiles for the cases of 0.2 ohm-cm and 1.5 ohm-cm N-type, epitaxial (collector) layer resistivity. The higher resistivity (1.5 ohm-cm) provides the lower time constant  $\tau = R_{ss} C_a$  for specified surface concentrations and junction depths. Figure 8 illustrates the comparison of two impurity profiles for the cases of  $x_C = 0.3$  and 0.4 micrometer. The shallower collector junction depth (0.3 micrometer) provides the lower time constant  $\tau = R_{ss} C_a$  for a fixed background concentration,  $C_B$ , and specified surface concentrations. Tables 1 and 2 summarize the comparison between the various design approaches for the microwave transistor impurity profile. The results indicate that shallow diffusions and high collector resistivity offer the largest improvement in  $f_{MAX}$ , which results in an increase in the maximum available unilateral power gain U(MAG) (see paragraph 4.2).

### 2.5 Neutral and Space-Charge Capacitance

The  $f_T$  can be increased by the reduction in base width; however, there is a tradeoff between improved  $f_T$  and increase in  $R_{ss}$ , as illustrated in Figure 5. The  $f_T$  may be improved through the selection of high impurity gradients at emitter-base and base-collector junctions. The emitter-base junction of a microwave transistor may be described

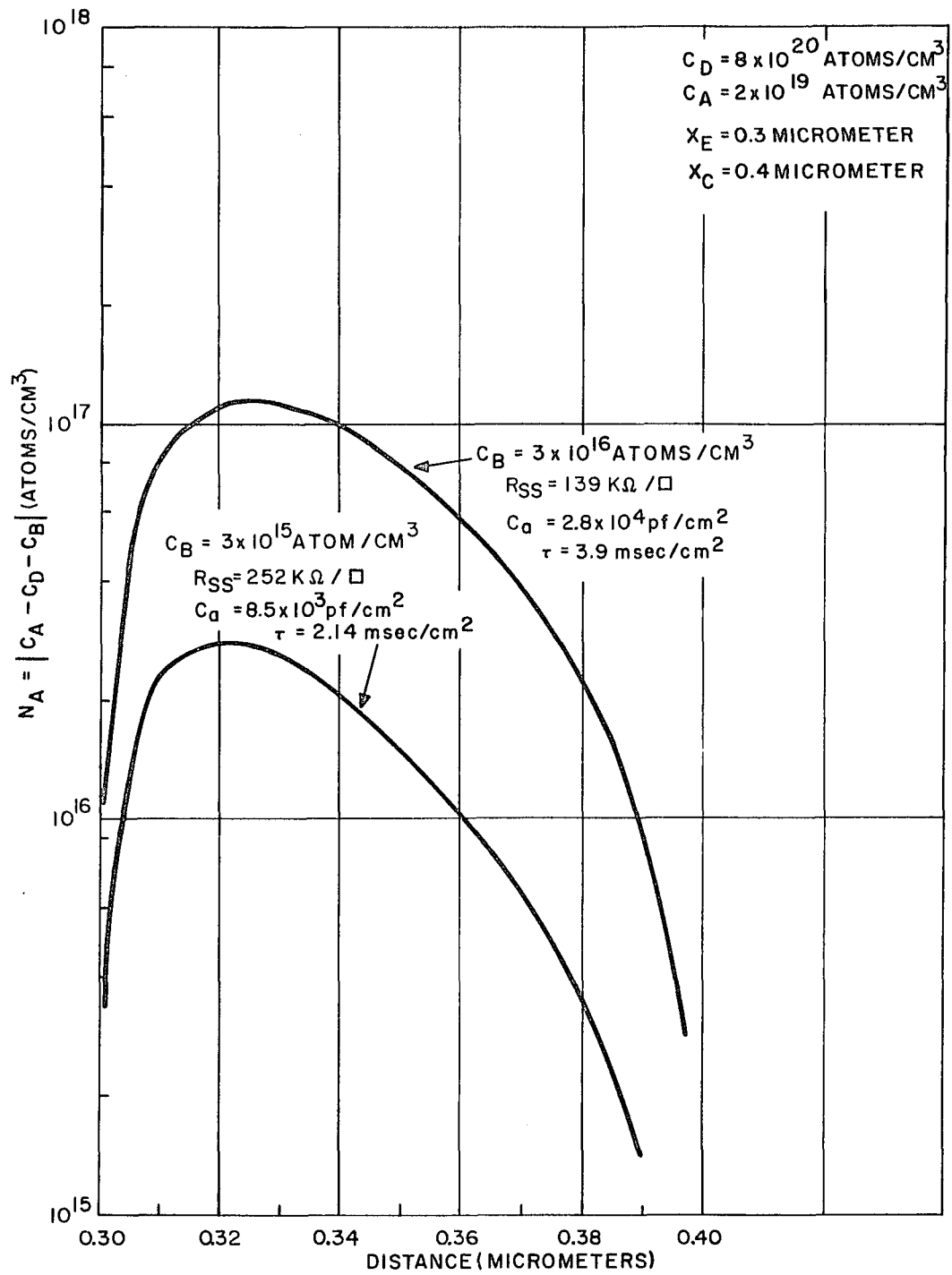


Figure 7. Effect of Background Concentration,  $C_B$ , on the Time Constant,  $\tau = R_{ss} C_a$

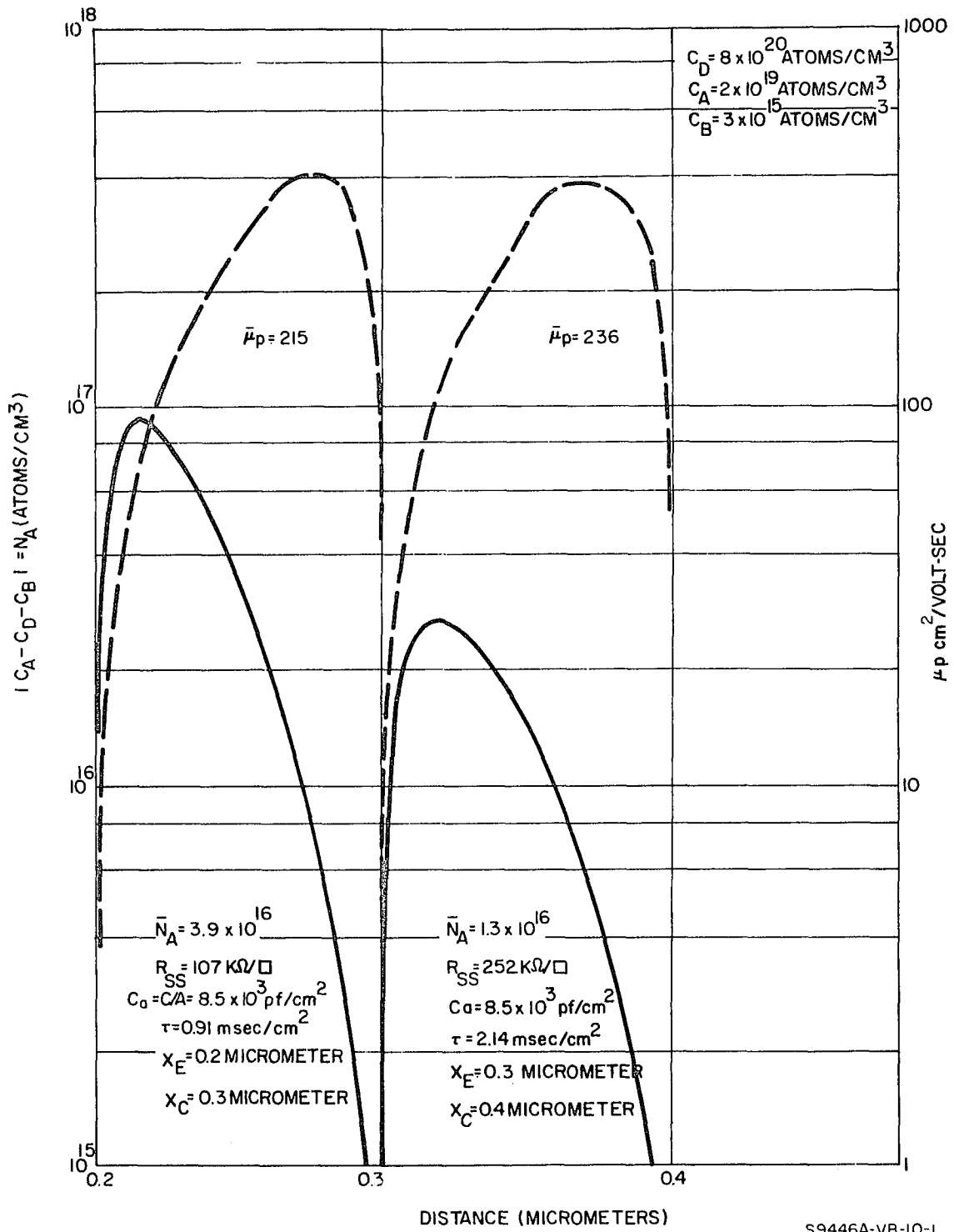


Figure 8. Effect of the Junction Depth on the Time Constant,

$$\tau = R_{ss} C_a$$

TABLE 1

COMPARISON OF MICROWAVE TRANSISTOR DESIGNS  
 FOR  $x_E = 0.3$  MICROMETER AND  $x_C = 0.4$   
 MICROMETER

$C_B$ (atoms/cm <sup>3</sup> )	$R_{ss}$ (ohms/square)	$C_a$ (pf/cm <sup>2</sup> )	$\tau = R_{ss} C_a$ (msec/cm <sup>2</sup> )
1 ohm-cm $3 \times 10^{15}$	252,000	$8.5 \times 10^3$	2.14
0.2 ohm-cm $3 \times 10^{16}$	139,000	$2.8 \times 10^4$	3.9

TABLE 2

COMPARISON OF MICROWAVE TRANSISTOR DESIGNS  
 FOR  $x_C - x_E = W = 0.1$  MICROMETER  
 AND  $C_B = 3 \times 10^{15}$  ATOMS/CM<sup>3</sup>

$x_C$ (micrometers)	$R_{ss}$ (ohms/square)	$C_a$ (pf/cm <sup>2</sup> )	$\tau = R_{ss} C_a$ (msec/cm <sup>2</sup> )
0.3	107,000	$8.5 \times 10^3$	0.91
0.4	252,000	$8.5 \times 10^3$	2.14

by a linear impurity gradient as illustrated in Figure 9. The space-charge capacitance of a linearly graded junction at equilibrium may be written as<sup>11</sup>

$$C_s = \left[ \frac{K_s^2 \epsilon_o^2 a_I}{12 (V + V_B)} \right]^{1/3} \quad (2-42)$$

where,  $a_I$  is the junction impurity gradient. For a graded p-n junction under sufficient forward bias (e. g., non-equilibrium conditions), the space-charge capacitance,  $C_s$ , as determined by equation 2-42 is not valid, because the effects of mobile minority carriers in the space-charge region must be considered in the analysis.<sup>12, 13</sup> The capacitance of the p-n junction for the case of forward bias may be written as

$$C_T = \frac{d}{dV} q \int_{-l/2}^{+l/2} p \, dx = \frac{d}{dV} q \int_0^{+l/2} (p+n) \, dx \quad (2-43)$$

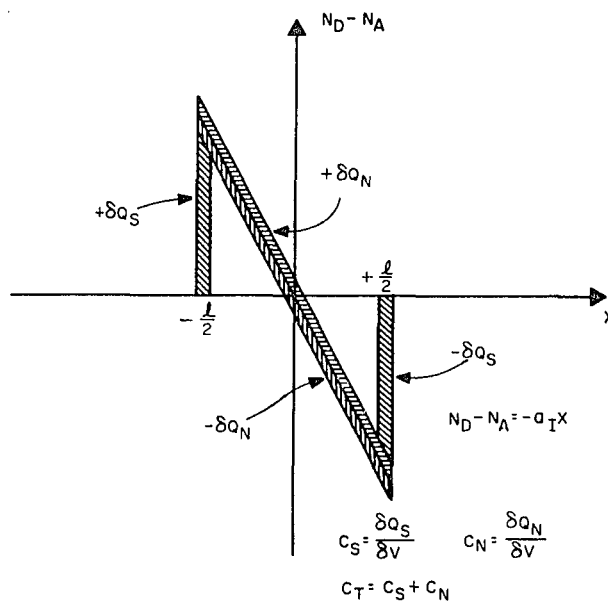
due to symmetrical injection. Equation 2-43 may be written as

$$\begin{aligned} C_T &= \frac{d}{dV} q \int_0^{+l/2} \left[ (p+n) + (N_A - N_D) \right] dx \\ &= \frac{d}{dV} 2q \int_0^{+l/2} p \, dx + \frac{d}{dV} \int_0^{+l/2} -\rho \, dx \\ &= \underbrace{C_n}_{\text{(neutral capacitance)}} + \underbrace{C_s}_{\text{(space-charge capacitance)}} \end{aligned} \quad (2-44)$$

<sup>11</sup>W. Shockley, Bell Syst. Tech. J., 28, 435 (1949).

<sup>12</sup>S. P. Morgan and F. M. Smits, Bell Syst. Tech. J. 39, 1573 (1960).

<sup>13</sup>D. P. Kennedy, Final Report No. 1., April 1, 1966 (Contract No. AF 19(628) - 5072).



S9446A-VB-9

Figure 9. Neutral and Space-Charge Capacitances in a Linearly Graded P-N Junction Under Forward Bias



since  $N_A - N_D = a_I x$  is independent of voltage and the space-charge  $\rho = q(p-n + N_D - N_A)$ . Thus, in a forward-biased p-n junction, the electrical capacitance arises from the storage of mobile charge carriers (neutral capacitance,  $C_n$ ) within the space-charge region and a redistribution of charges within the electrical double-layer (space-charge capacitance,  $C_s$ ). The neutral capacitance depends upon the width of the space-charge region as indicated in Figure 9. A large impurity gradient,  $a_I$ , will reduce the neutral capacitance effects through a decrease in the width  $\ell$ ; however, the space-charge capacitance will increase as indicated by equation 2-42. Table 3 illustrates the impurity gradients at the emitter-base and base-collector junctions for various impurity profiles. Figure 10 illustrates the variation of  $C_n$  and  $C_s$  with applied forward voltage for various impurity profiles (i. e., impurity gradients) in the emitter-base junction. The results indicate that a high impurity gradient will reduce the neutral capacitance, which is the dominant effect at the high current densities (i. e.,  $\sim 10^3$  amperes/cm<sup>2</sup>) encountered in the microwave transistor operation. The space-charge capacitance will increase; however, it is insignificant at these current levels. Equation 3-9 illustrates the importance of a low  $r_e C_T$  time constant to reduce the emitter-to-collector transit time and thus, improve the  $f_T$  of the transistor.

TABLE 3

## IMPURITY GRADIENTS IN A MICROWAVE TRANSISTOR

$$C_D = 8 \times 10^{20}; C_A = 2 \times 10^{19}; C_B = 3 \times 10^{15}$$

$x_E, x_C$ (micrometers)	$a_I$ (emitter-base) ( $CM^{-4}$ )	$a_I$ (collector-base) ( $CM^{-4}$ )
$x_E = 0.3$	$2.5 \times 10^{22}$	$1.3 \times 10^{21}$
$x_C = 0.4$		
$x_E = 0.2$	$1.0 \times 10^{23}$	$2.0 \times 10^{21}$
$x_C = 0.3$		

## 2.6 Collector Junction Displacement

The linearly graded base-collector junction of the microwave transistor is illustrated in Figure 11. At equilibrium, the depletion layer width is given by<sup>11</sup>

$$x_d = x_2 - x_1 = \left[ \frac{12K_s \epsilon_o (V_C + V_B)}{q a_I} \right]^{1/3} \quad (2-45)$$

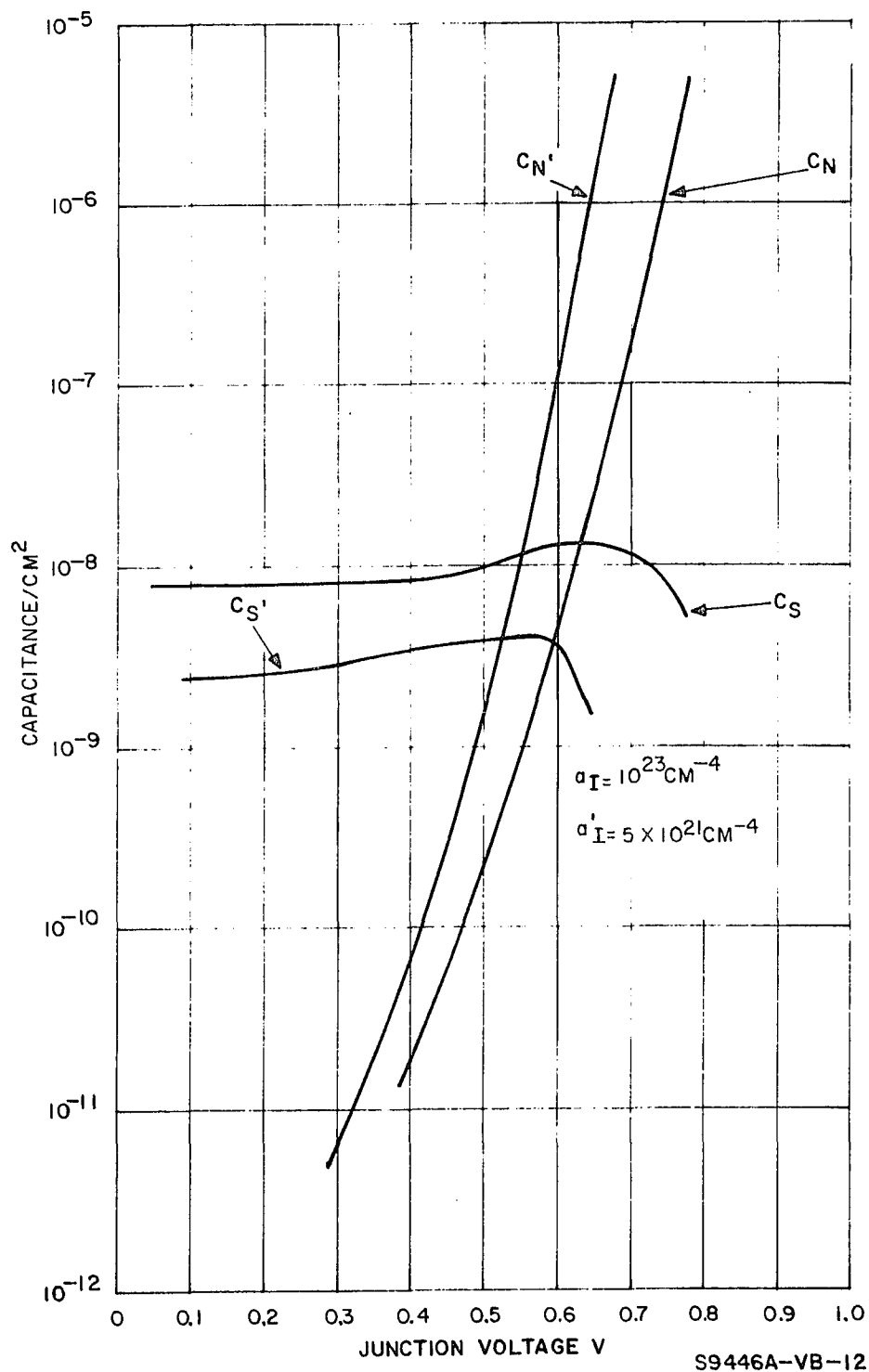


Figure 10. Effect of Impurity Gradient on the Neutral and Space-Charge Capacitances in a Linearly Graded P-N Junction Under Forward Bias

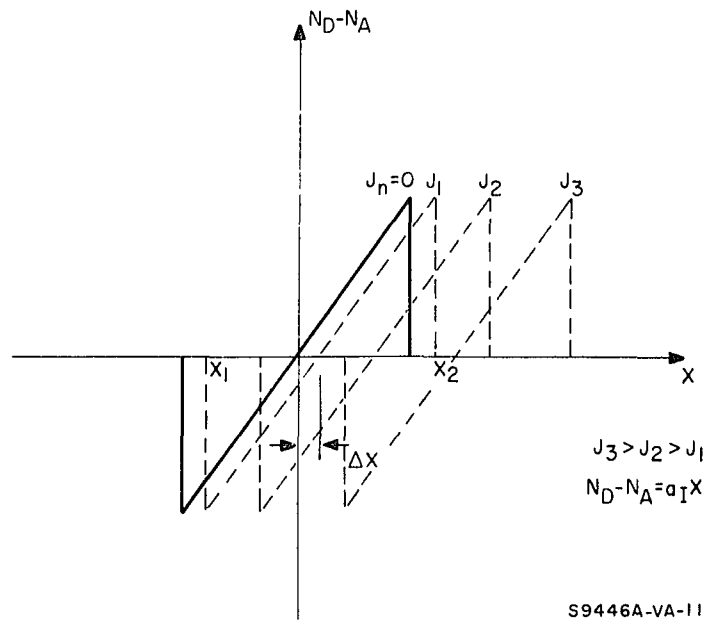


Figure 11. Displacement of the Space-Charge Region  
in a Linearly Graded Base-Collector P-N Junction  
With Increasing Current Density

where,  $V_C$  is the collector-base voltage. In a non-equilibrium situation, where there is current flow through the depletion layer, the space-charge density is modified by the expression

$$\begin{aligned}\rho(x) &= q a_I x - \frac{J_n}{V_L} \\ &= q a_I(x - \Delta x)\end{aligned}\tag{2-46}$$

where  $\Delta x = J_n / q V_L a_I = n / a_I$  is the linear translation of the effective junction. The injected electron density,  $n$ , uniformly depresses the space-charge region. The higher the impurity gradient,  $a_I$ , the smaller the shift,  $\Delta x$ , in the junction for a specified current density. The new boundaries in the non-equilibrium case are given as

$$\begin{aligned}x_2 &= x_d + \Delta x \\ x_1 &= x_d - \Delta x.\end{aligned}\tag{2-47}$$

Figure 11 illustrates the displacement of the space-charge region with an increase in current density.<sup>14</sup> The displacement of the depletion layer boundaries results in an increase in the base-transit time, through an increase in the electrical base width,  $W$ ; however, the

---

<sup>14</sup>C. T. Kirk Jr., IRE Trans. on Electron Devices, ED-9, 164 (1961).  
R. Lloyd, IEEE Trans. on Electron Devices, ED-13, 991 (1966).  
Kirk and Lloyd conclude that the effective junction moves in a linearly graded junction in contrast to an abrupt junction.

collector transit time remains unchanged. At small values of the applied collector voltage,  $V_C$ , the electric field is insufficient to transport the electrons at the terminal or limiting velocity,  $V_L$ . Thus, at small values of junction voltage, the space-charge region width,  $x_d$  will be sensitive to displacement. Once the terminal velocity is attained, the space-charge region undergoes a linear translation in the direction to increase the effective electrical base width of the transistor.

## CHAPTER III

### MICROWAVE TRANSISTOR SMALL-SIGNAL EQUIVALENT CIRCUIT

#### 3.1 Introduction

The switching or large-signal characteristics of the microwave transistor have been investigated with a non-linear, semi-distributed model of the transistor and computer calculations.<sup>1</sup> The small-signal characteristics have also been studied with a T-equivalent circuit and computer calculations to determine the h-parameters of the microwave transistor.<sup>2</sup> In this chapter, the small-signal characteristics of the microwave transistor will be analyzed with a T-equivalent circuit suitably modified to account for package parasitics.

#### 3.2 Base Charging Circuit Time Constant, $r_b' C_c$

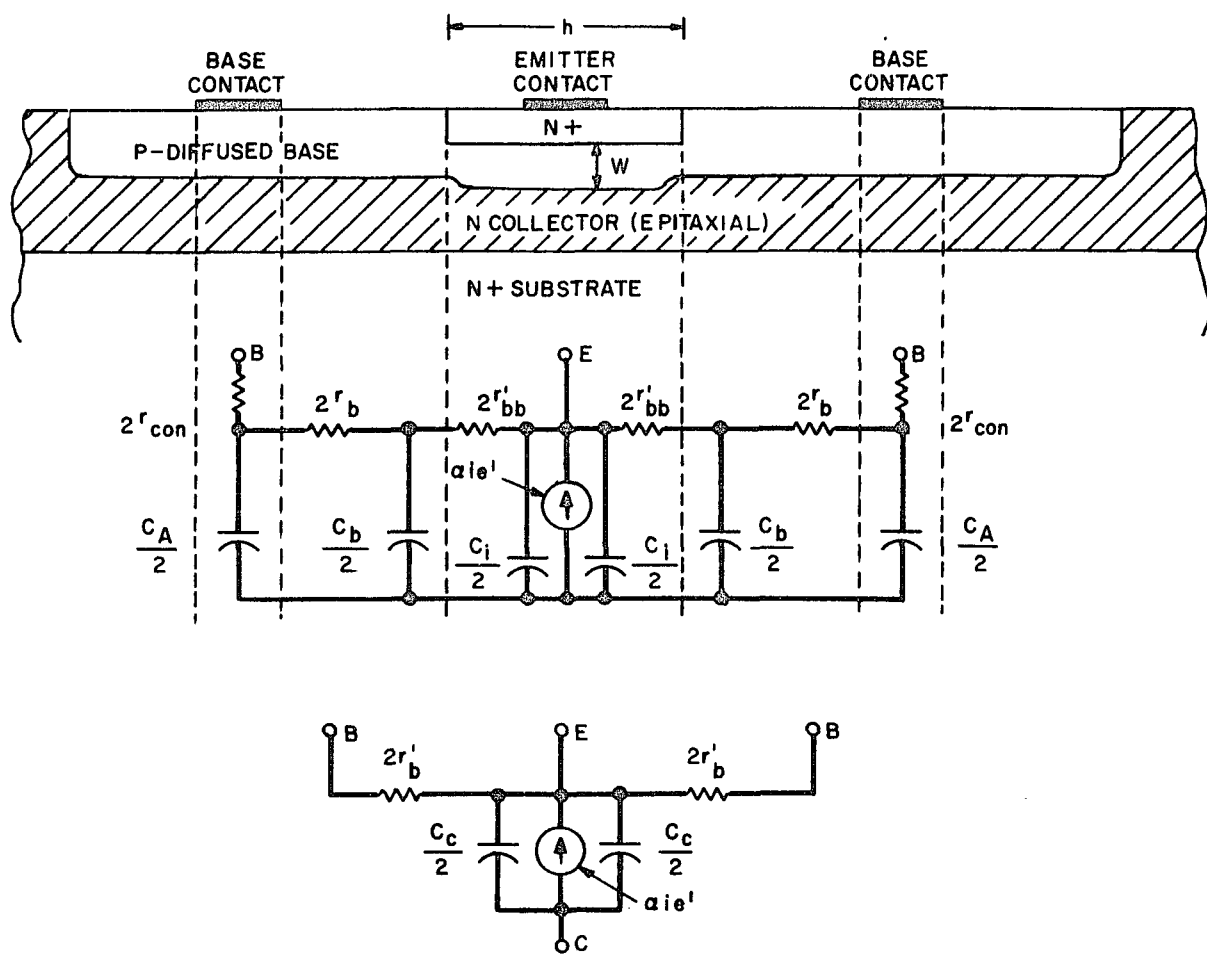
The base charging circuit of the microwave transistor may be represented by the semi-distributed RC network<sup>3</sup> illustrated in Figure 12. Figure 12 illustrates a cross-sectional view of a single-emitter

---

<sup>1</sup>H. N. Ghosh, et. al., Solid-State Electronics, 10, 705 (1967).

<sup>2</sup>W. E. Beadle, et. al., IEEE Trans. on Electron Devices, ED-16, 125 (1969).

<sup>3</sup>R. Edwards and R. L. Pritchett, NEREM Rec., 246 (Boston, Mass., 1965).



S9234A-VA-9-1

Figure 12. Cross Section of a Double Base Strip, Single Emitter Strip Microwave Transistor. Base Charging Circuit Time Constant,  $r'_b C_c$ , Equivalent Circuit



and double-base strip construction for the microwave transistor. The base charging circuit is decomposed into lumped RC sections that represent the signal current flow into the base region of the transistor. The emitter strip width is designated by the symbol "h" and the electrical base width by the symbol "W". The various elements in the base charging circuit are described as follows:

- a.  $r_{\text{con}}$  = contact resistance associated with the double base strips.
- b.  $r_b$  = interstripe base resistance associated with current flow between the base contacts and the emitter strip region.
- c.  $r'_{\text{bb}}$  = transverse base resistance associated with current flow beneath the emitter strip.
- d.  $C_i$  = base-collector capacitance directly beneath the emitter strip.
- e.  $C_b$  = base-collector capacitance between the edges of the emitter strip and the base contacts.
- f.  $C_A$  = base-collector capacitance (not including  $C_i$  and  $C_b$ ) including the bonding pad and side-wall capacitances.

The current generator  $\alpha_i'$ , with the collector and base terminals of the transistor short-circuited (ac), sees an input impedance given as

$$Z \doteq \frac{r'_b}{1 + j\omega r'_b C_c} \quad (3-1)$$

where second and higher-order frequency terms have been neglected in the analysis. The lumped elements in equation 3-1 are defined by the expressions

$$r'_b = r_{con} + r_b + r'_{bb} \quad (3-2)$$

$$r'_b C_c = r_{con} (C_i + C_b + C_A) + (r'_{bb} + r_b) C_i + r_b C_b \quad (3-3)$$

Several comments are in order regarding the  $r'_b C_c$  representation of the base-charging circuit. First, the element  $r'_b$  is the total base resistance, which is the sum of the contact resistance,  $r_{con}$ , the interstrip resistance,  $r_b$ , and the transverse base resistance beneath the emitter strip,  $r'_{bb}$ . Second, the capacitance,  $C_c$ , is only defined through equations 3-2 and 3-3, and as such, there is no direct, one-to-one correspondence with device geometry for this circuit element. Third, equation 3-3 indicates that the total base-collector capacitance ( $C_i + C_b + C_A$ ) is multiplied by the contact resistance,  $r_{con}$ . Thus, it is necessary to minimize the contact resistance associated with the metal-semiconductor contact to reduce the  $r'_b C_c$  time constant.

### 3.3 The T-Equivalent Circuit

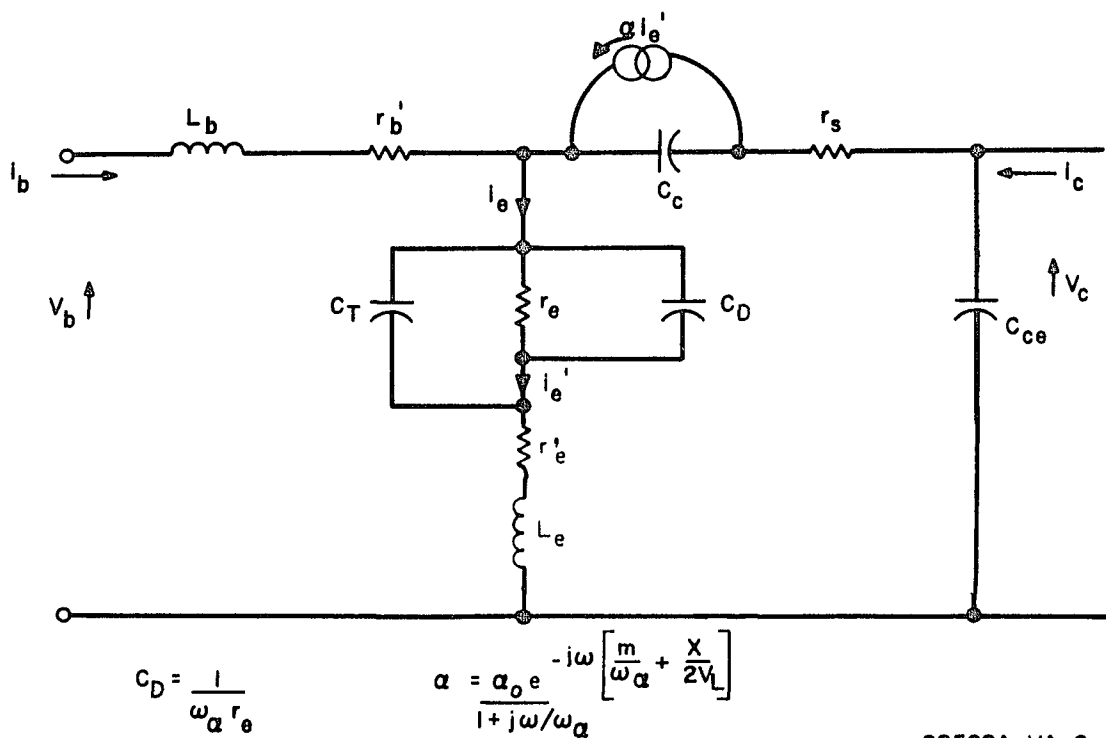
The small-signal T-equivalent circuit model of the microwave transistor is illustrated in Figure 13. The model includes the following extrinsic elements:

- a. Emitter space-charge and neutral capacitances;  $C_T = C_s + C_n$ .
- b. Base and emitter lead inductances;  $L_b$  and  $L_e$ .
- c. Collector series resistance;  $r_s$ .
- d. Emitter contact or series resistance;  $r'_e$ .
- e. Time delay associated with the transit time of carriers across the collector depletion layer;  $\frac{x}{2V_L}$ .

The current generator, previously discussed in paragraph 3.2, pertains to only that portion of the emitter current that flows by diffusion and drift mechanisms. The displacement current that flows through  $C_T$  is not amplified in the equivalent circuit shown in Figure 13. A simplified representation of the intrinsic input admittance is used in which the diffusion capacitance,  $C_D = 1/r_e \omega \alpha'$ , is shunted by the incremental forward resistance,  $r_e$ . A more exact analysis would include the effects of the built-in electric field and the distributed nature of the carrier transport through the base region.<sup>4</sup> The current amplification factor may be approximated by the expression

---

<sup>4</sup>R.P. Abraham, IRE Trans. on Electron Devices, ED-7, 59 (1960).



S8528A-VA-8-1

Figure 13. Small Signal Lumped T-Equivalent Circuit of the Microwave Transistor in the Common-Emitter Configuration

$$\alpha = \frac{\alpha_o e^{-j\omega \left[ \frac{m}{\omega_\alpha} + \frac{x}{2V_L} \right]}}{1 + j\omega/\omega_\alpha} \quad (3-4)$$

in which a single pole and excess linear phase shift describes the distributed properties of the transistor with a constant electric field in the base region.<sup>5</sup> The excess phase shift,  $m$ , is attributed to the drift-diffusion mechanism of carrier transport in the base region, while the time delay,  $x/2V_L$ , describes the carrier transport through the collector depletion layer. (The  $x$  is the width of the collector depletion layer, and  $V_L$  is the maximum scatter-limited velocity of carriers in the depletion layer.) If the impurity distribution in the base region is approximated by an exponential distribution, then the alpha cut-off frequency,  $\omega_\alpha$ , and excess phase shift,  $m$ , may be related to each other through an electric field parameter  $\eta = \frac{1}{2} \ln N_{EB}/N_{BC} = -\xi W/2k_B T$ , where  $N_{EB}$  and  $N_{BC}$  represent the impurity concentrations at the emitter and collector junctions, respectively. Table 4 illustrates the effect of varying the impurity distribution in the base region upon these parameters.<sup>6</sup> The  $\omega_\alpha$  is described by a normalizing parameter

<sup>5</sup>D. E. Thomas and J. L. Moll, Proc. IRE, 46, 1177 (1958).

<sup>6</sup>V. Uzunoglu and M.H. White, Semiconductor Products and Solid State Technology, 1, Feb. (1965).

TABLE 4

EFFECT OF THE BUILT IN ELECTRIC FIELD  
IN THE BASE REGION UPON THE  $\omega_\alpha$  and m OF A MICROWAVE  
TRANSISTOR.

$\frac{\omega_\alpha}{\omega_D}$	$\eta = \frac{1}{2} \ln N_{EB}/N_{BC} = -\frac{1}{2} q \frac{\xi W}{k_B T}$	m radians (degrees)
29.5	6	1.35 (77)
23.2	5	1.17 (67)
17.6	4	1.00 (57)
12.6	3	0.82 (47)
8.3	2	0.61 (35)
4.9	1	0.40 (23)
2.44	0	0.22 (12.6)

$\omega_\alpha$  - alpha cut-off frequency for the common base transistor

$\omega_D = \bar{D}_n/W^2$  - diffusion cut-off frequency

$\bar{D}_n$  - average diffusion constant for electrons

W - electrical base width

$\eta$  - electric field parameter

m - excess phase shift

$N_{EB}, N_{BC}$  - emitter-base and base-collector impurity concentrations

$\xi$  - internal constant electric field

called the diffusion frequency;  $\omega_D = \bar{D}_n/W^2$ , where  $\bar{D}_n$  is the average minority carrier (electrons for a npn device) diffusion constant, and  $W$  is the electrical base width of the transistor. At low injection levels, the effect of the impurity gradient in the base region in altering the internal electric field is important; however, as the current density increases, the mobile carriers tend to compensate the built-in electric field (wash-out effect).

### 3.4 Current-Gain Bandwidth Product, $f_T$

The microwave transistor in the common-emitter configuration is examined by ac short-circuiting the output terminals and evaluating the ratio of collector-to-base currents. From Figure 13, with second and higher-order frequency terms neglected

$$h_{fe}(\omega) = \frac{i_c}{i_b} = h_{fe_o} \frac{1 - j\omega T_d}{1 + j\omega/\omega_o} = h_{fe_o} \frac{e^{-j\omega T_d}}{1 + j\omega/\omega_o} \quad (3-5)$$

where,  $h_{fe_o} = \frac{\alpha_o}{1 - \alpha_o}$  is the low frequency common-emitter short-circuit current gain. The time delay,  $T_d$ , and corner frequency,  $\omega_o$ , are given as

$$T_d = \frac{m}{\omega_o} + \frac{x}{2V_L} + \frac{C_c}{\alpha_o} (r_e + r'_e) \quad (3-6)$$

$$\frac{1}{\omega_o} = \frac{1}{1 - \alpha_o} \left[ \frac{1 + \alpha_o m}{\omega_\alpha} + r_e (C_T + C_c) + \frac{\alpha_o x}{2V_L} + C_c (r'_e + r_s) \right]. \quad (3-7)$$

A convenient method to characterize a high frequency transistor is in terms of the current-gain bandwidth product,  $f_T$ .<sup>7</sup> Examination of equation 3-5 for frequencies  $\omega \gg \omega_o$  shows,

$$\omega_T = 2\pi f_T = h_{fe_o} \omega_o = \frac{1}{T_{ec}} \quad (3-8)$$

where,  $T_{ec}$  is the emitter-to-collector transit time, which comprises the following terms:

$$T_{ec} = \frac{1 + \alpha_o m}{\alpha_o \omega_\alpha} + \frac{x}{2V_L} + \frac{r_e}{\alpha_o} (C_T + C_c) + \frac{C_c}{\alpha_o} (r'_e + r_s).$$

(base transit time)	+ (collector depletion layer transit time)	+ (emitter time constant)	+ (collector time constant)
------------------------	---	---------------------------------	-----------------------------------

(3-9)

The  $f_T$  represents the frequency at which the common-emitter short-circuit current gain is unity. If the emitter-to-collector transit time,  $T_{ec}$ , is plotted versus  $1/I_C$ , where  $I_C$  is the collector current for a fixed collector voltage  $V_{CE}$ , then the slope of the curve will yield

<sup>7</sup>J.M. Early, Proc. IRE, 46, 1924 (1958). Equation 3-9 differs from Early's result with the additional time constant  $(r'_e + r_s) C_c$ .



information regarding the sum of the capacitances,  $C_T + C_c$ ,<sup>8</sup> at low current levels. As the current density increases in the microwave transistor, the  $C_T$  increases due to the neutral capacitance<sup>9,10</sup> effect discussed in Chapter II. The storage of mobile charge carriers in the emitter-base depletion layer is very important at increased current levels.

---

<sup>8</sup>Since  $r_e = \alpha \frac{kT}{qI_c}$ , the slope of the curve at low current levels is seen to be  $(C_T + C_c) \frac{kT}{q}$ .

<sup>9</sup>S.P. Morgan and F.M. Smits, Bell Syst. Tech. J., 39, 1573 (1960).

<sup>10</sup>The formulation of the equivalent circuit and equation 3-9 assumes that the excess injected carrier concentration at the edge of the collector depletion layer is zero. If the injected concentration is considered, then an additional term of  $W/V_L$  must be added to the base transit time to account for the additional time required to store this charge in the neutral base region. See, C.T. Kirk, IRE Trans. on Electron Devices, ED-9, 164 (1961).

CHAPTER IV  
SCATTERING PARAMETER FORMULATION

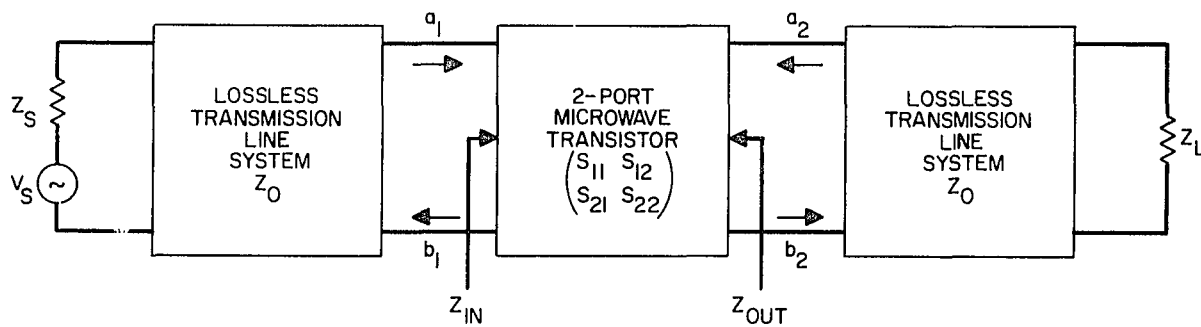
4.1 Introduction to S-(Scattering) Parameters

The generalized scattering or s-parameters<sup>1</sup> are described by a set of variables ( $a_i, b_i$ ), which represent a normalized set of complex voltage waves incident on the  $i^{\text{th}}$  port of a network as shown in Figure 14. These variables are defined in terms of the terminal voltages and currents and a reference  $Z_o$  (positive, real, line impedance) as follows:

$$\begin{aligned}
 a_1 &= \frac{v_1 + i_1 Z_o}{2\sqrt{Z_o}} &= & \frac{\text{voltage wave incident on port 1}}{\sqrt{Z_o}} \\
 a_2 &= \frac{v_2 + i_2 Z_o}{2\sqrt{Z_o}} &= & \frac{\text{voltage wave incident on port 2}}{\sqrt{Z_o}} \\
 b_1 &= \frac{v_1 - i_1 Z_o}{2\sqrt{Z_o}} &= & \frac{\text{voltage wave reflected from port 1}}{\sqrt{Z_o}} \\
 b_2 &= \frac{v_2 - i_2 Z_o}{2\sqrt{Z_o}} &= & \frac{\text{voltage wave reflected from port 2}}{\sqrt{Z_o}}
 \end{aligned}$$

---

<sup>1</sup>K. Kurokawa, IEEE Trans. on Microwave Theory and Techniques, MTT-13, 194 (1965).



S9234A-VA-1

Figure 14. Two-Port Microwave Transistor  
(S-Parameter Characterization)

The linear equations which describe the two-port microwave transistor are written as

$$\begin{aligned} b_1 &= s_{11} a_1 + s_{12} a_2 \\ b_2 &= s_{21} a_1 + s_{22} a_2 \end{aligned} \quad (4-2)$$

where the coefficients are called the s-(scattering) parameters.

Specifically, these parameters can be written in the form:

$$\begin{aligned} s_{11} &= \left. \frac{b_1}{a_1} \right|_{a_2=0} = \text{input reflection coefficient} = \frac{v_1 - i_1 Z_o}{v_1 + i_1 Z_o} = \frac{Z_{in} - Z_o}{Z_{in} + Z_o} \\ &\quad \text{with the output terminated} \\ &\quad \text{in a matched load } (Z_L = Z_o) \\ s_{21} &= \left. \frac{b_2}{a_1} \right|_{a_2=0} = \text{forward insertion gain} = \frac{-2Z_o i_2}{v_1 + i_1 Z_o} = -\gamma_f \frac{i_2}{i_1} \\ &\quad \text{with the output terminated} \\ &\quad \text{in a matched load } (Z_L = Z_o) \\ s_{12} &= \left. \frac{b_1}{a_2} \right|_{a_1=0} = \text{reverse insertion gain} = \frac{-2Z_o i_1}{v_2 + i_2 Z_o} = -\gamma_r \frac{i_1}{i_2} \\ &\quad \text{with the input terminated} \\ &\quad \text{in a matched load } (Z_s = Z_o) \\ s_{22} &= \left. \frac{b_2}{a_2} \right|_{a_1=0} = \text{output reflection coefficient} = \frac{v_2 - i_2 Z_o}{v_2 + i_2 Z_o} = \frac{Z_{out} - Z_o}{Z_{out} + Z_o} \\ &\quad \text{with the input terminated in} \\ &\quad \text{a matched load } (Z_s = Z_o) \end{aligned} \quad (4-3)$$

where  $\gamma_f = \frac{2Z_o}{Z_{in} + Z_o}$  and  $\gamma_r = \frac{2Z_o}{Z_{out} + Z_o}$  are the forward

and reverse current transmission factors of the microwave transistor.

## 4.2 S-Parameter Formulation in Terms of Device Parameters

The s-parameters of the microwave transistor were discussed briefly in paragraph 4.1. If the output of the microwave transistor is terminated in  $Z_o$ , the characteristic impedance of a properly terminated transmission line, then the ratio of collector-to-base currents becomes

$$T_f(\omega) = \frac{i_c}{i_b} = h_{fe_o} \frac{e^{-j\omega T_d}}{1 + j\omega/\omega_1} \quad (4-4)$$

where the new corner frequency is given as

$$\omega_1 = \frac{\omega_o}{1 + \frac{\omega_o C_c Z_o}{1 - \alpha_o}} \quad (4-5)$$

Refer to paragraph 3.3 for a discussion of the T-equivalent circuit and the definition of  $\omega_o$ . For frequencies  $\omega \gg \omega_1$ , the current transfer ratio  $T_f(\omega)$  can be written as

$$T_f(\omega) = \frac{\omega'_T}{j\omega} e^{-j\omega T_d} = \frac{\omega'_T}{\omega} e^{-j(\pi/2 + \omega T_d)} \quad (4-6)$$

where,

$$\omega'_T = \frac{\omega_T}{1 + \frac{\omega_T C_c Z_o}{\alpha_o}} \quad (4-7)$$

is a reduced current-gain bandwidth product. The effect of terminating the transistor in a load,  $Z_o$ , is to reduce the current-gain bandwidth product of the amplifier. The input impedance,  $Z_{in}$ , of the microwave transistor may be obtained from the T-equivalent circuit in Chapter III and equation 4-6, with the result that

$$\begin{aligned} Z_{in} &= r'_b + r'_e + r_e + \omega'_T L_e + j\omega (L_e + L_b) + \frac{\omega'_T (r_e + r'_e)}{j\omega} \\ &= R + j\omega L + \frac{1}{j\omega C} \end{aligned} \quad (4-8)$$

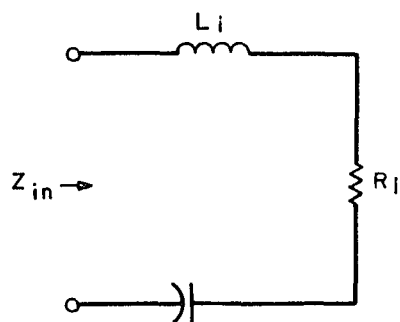
assuming second and higher-order frequency terms are negligible and that the phase shift  $\omega T_d \ll 1$ .<sup>2</sup> Thus, the input equivalent circuit of the microwave transistor is a series RLC circuit, as shown in Figure 15(a). The input reflection coefficient for the common-emitter microwave transistor amplifier is given as

$$s_{11} = s_{ie} = \frac{Z_{in} - Z_o}{Z_{in} + Z_o} \quad (4-9)$$

which is shown qualitatively in Figure 15(a), using the Smith Chart representation, with the input impedance normalized to the transmission line impedance,  $Z_o$ . At low frequencies, the input impedance appears capacitive; however, as the frequency is increased, the

---

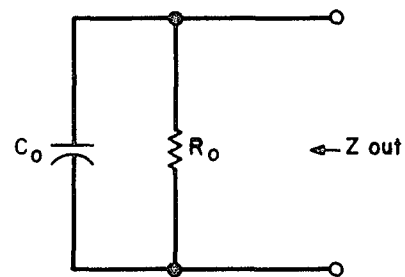
<sup>2</sup>If  $\omega T_d < 1$ , then the  $Z_{in} = r'_b + r'_e + r_e + \omega'_T [L_e - (r_e + r'_e) T_d] + j\omega [L_b + L_e (1 - \omega'_T T_d)] + \frac{\omega'_T (r_e + r'_e)}{j\omega}$



$$L_i \doteq L_e + L_b \quad C_i = \frac{1}{\omega_T'(r_e + r_e')}$$

$$R_i = r_b' + r_e + \omega_T' L_e + r_e'$$

a) INPUT EQUIVALENT CIRCUIT



$$C_o \doteq C_{ce} + \frac{C_c}{1 + \alpha_m}$$

$$R_o \doteq \frac{1}{\omega_T C_c}$$

b) OUTPUT EQUIVALENT CIRCUIT

S8528A-VA-3-1

Figure 15. Small-Signal Equivalent Circuits of the Common-Emitter Microwave Transistor at Input and Output Ports

parasitic lead inductances dominate. The intersection of  $Z_{in}$  with the real axis provides a convenient method to evaluate the microwave transistor parameters since

$$\text{Re} [ Z_{in} (\omega = \omega_{res.}) ] = R = r'_b + r'_e + r_e + \omega'_T L_e \quad (4-10)$$

and the resonant frequency is given as

$$\omega_{res.} = \sqrt{\frac{\omega'_T (r_e + r'_e)}{L_e + L_b}} \quad (4-11)$$

The forward insertion gain,  $s_{21} = s_{fe}$ , for the common-emitter microwave transistor may be evaluated with equations 4-6 and 4-8, together with equation 4-3. Thus, for frequencies  $\omega \gg \omega_1$ , we may write the magnitude and phase of the insertion gain as

$$\begin{aligned} |s_{fe}| &= \frac{2 Z_o \omega'_T}{\omega \sqrt{(R + Z_o)^2 + (\omega L - 1/\omega C)^2}} \\ &= \frac{2 Z_o \omega'_T}{\omega (R + Z_o)} \end{aligned} \quad (4-12)$$

$$\angle s_{fe} = \pi/2 - \tan^{-1} \left[ \frac{\omega L - 1/\omega C}{R + Z_o} \right] - \tan^{-1} \omega T_d \quad (4-13)$$

which is shown qualitatively in Figure 16(c), with a Polar Plot representation. The transducer gain,  $G_T = |s_{fe}|^2$ , is the power gain of the microwave transistor amplifier operating in a system of characteristic impedance,  $Z_o$ . Equation 4-12 indicates that the



transducer gain may be expected to fall off at the rate of 6 dB/octave, with the 0 dB intercept a measure of the  $f_T$  of the microwave transistor.

The output impedance of the microwave transistor is determined by the termination of the input in the characteristic line impedance,  $Z_o$ . The output impedance may be written in the form

$$Z_{out} = \frac{R_o}{1 + j\omega R_o C_o} \quad (4-14)$$

where,

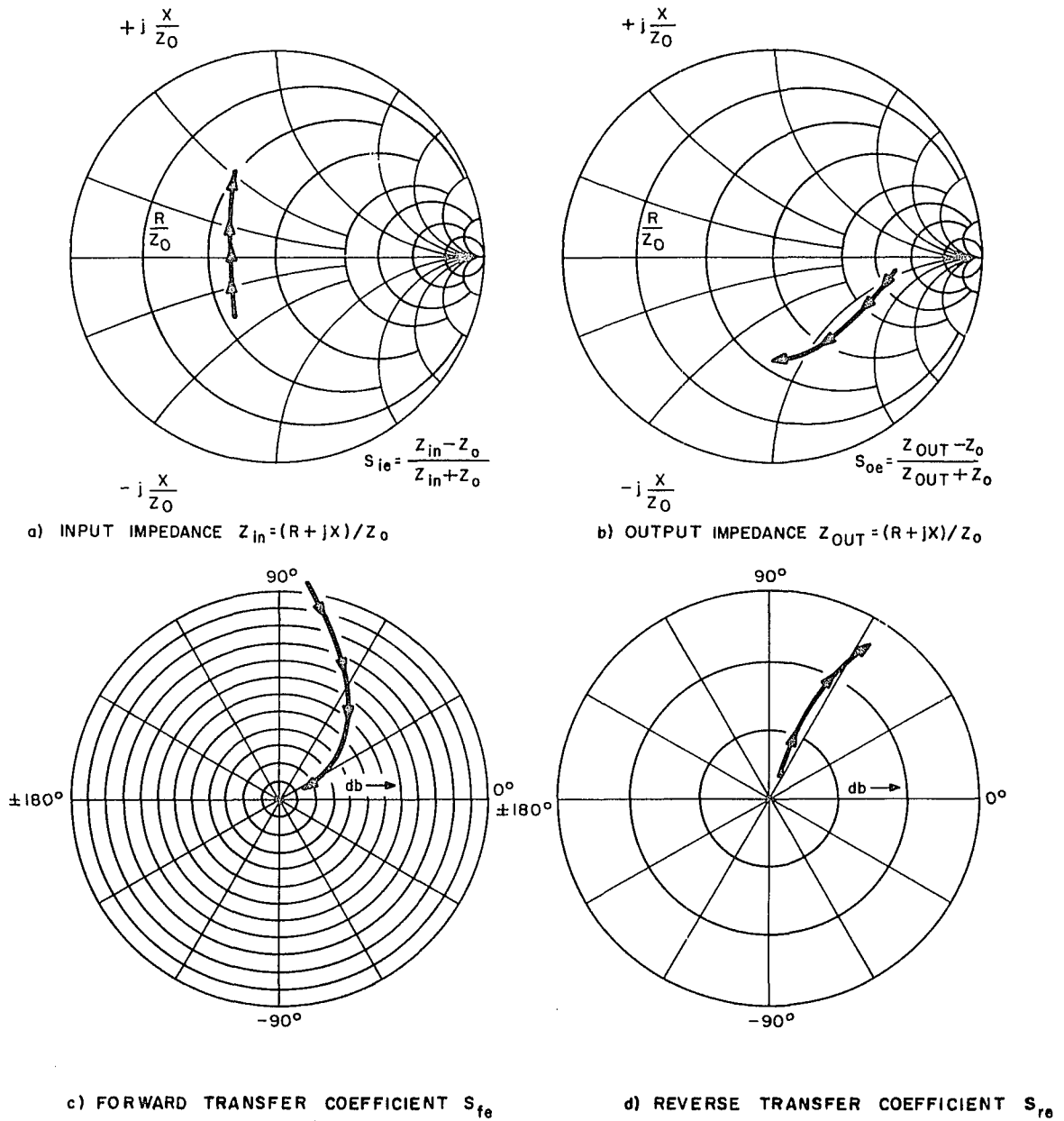
$$R_o = \frac{1}{\omega_T C_c} \quad (4-15)$$

$$C_o = C_{ce} + \frac{C_c}{1 + \alpha_m} \quad (4-16)$$

The effects of the emitter lead inductance and second and higher-order frequency terms are neglected in the formulation of equation 4-14. The output of the microwave transistor is a parallel  $R_o C_o$  circuit, as shown in Figure 15(b). The output reflection coefficient,  $s_{22} = s_{oe}$ , for the common emitter amplifier is given as

$$s_{22} = s_{oe} = \frac{Z_{out} - Z_o}{Z_{out} + Z_o} \quad (4-17)$$

which is shown qualitatively in Figure 16(b), using the Smith Chart representation with the output impedance normalized to the transmission line impedance,  $Z_o$ .



S8528A-VE-9

Figure 16. S-Parameters Versus Increasing Frequency for a Common-Emitter Microwave Transistor

To determine the reverse insertion gain,  $s_{12} = s_{re}$ , for the common-emitter microwave transistor, the reverse current transfer ratio,  $T_r(\omega)$ , is evaluated for the input terminated in  $Z_o$ . Neglecting the second and higher-order frequency terms, the transfer ratio becomes

$$T_r(\omega) = \frac{i_b}{i_c} \doteq \frac{(r_e + r'_e)(1 + j\omega L_e / r_e + r'_e)}{(r_e + r'_e + r'_b + Z_o)(1 + j\omega T_o)} \quad (4-18)$$

where,

$$T_o \doteq \frac{L_e + L_b}{r_e + r'_e + r'_b + Z_o} + \frac{1}{\omega_\alpha} + C_T r_e \quad (4-19)$$

The reverse insertion gain is determined from equations 4-14, 4-18 and 4-3. The magnitude and phase of  $s_{re}$  may be written as

$$|s_{re}| \doteq \frac{2(r_e + r'_e) Z_o \sqrt{1 + \omega L_e / r_e + r'_e}^2}{(R_o + Z_o)(r_e + r'_e + r'_b + Z_o) \sqrt{1 + (\omega T_o)^2}} \quad (4-20)$$

$$\angle s_{re} \doteq \tan^{-1} \frac{\omega L_e}{r_e + r'_e} - \tan^{-1} \omega T_o \quad (4-21)$$

which is shown qualitatively in Figure 16(d), with a Polar Plot representation. The emitter lead inductance,  $L_e$ , and contact resistance,  $r'_e$ , must be reduced to lower the reverse insertion gain. In general, if the lead inductance is small, the insertion gain can be reduced by operating the transistor at high current levels. If the lead inductance is large, the insertion gain increases at the rate of 6 dB/octave.

### 4.3 Maximum Unilateral Gain U(MAG) and $f_{MAX}$

The transducer gain,  $G_T = |s_{fe}|^2$ , for a common-emitter microwave transistor has been discussed for a transmission line of characteristic impedance  $Z_o$ . With equations 4-6 and 4-3, we may write the frequency at which  $G_T$  is unity as

$$\omega_{trans} = \omega_T' \sqrt{\gamma_f} \quad (4-22)$$

where  $\omega_T'$  is defined by equation 4-7 and  $\gamma_f$  by equations 4-3 and 4-8.

The  $\omega_{trans}$  is a measure of the  $f_T$  of a microwave transistor, since in low power devices, the  $\gamma_f$  is close to unity, while the  $\omega_T'$  is nearly the  $\omega_T$  of the transistor. Figure 17 illustrates the variation of  $G_T$  with frequency for a common-emitter microwave transistor amplifier.

Although the current gain of the transistor may become less than unity at higher frequencies, power gain is still achieved, since there is a difference between the input and output impedance levels in the device. Thus, a more meaningful description of the microwave transistor from the standpoint of power amplification is the specification of the maximum frequency at which power amplification is obtained. To determine this frequency, the maximum available unilateral transducer power gain, U(MAG), is calculated under the assumption that  $s_{re} = 0$ . The U(MAG) may be written as<sup>3</sup>

---

<sup>3</sup>R. L. Anderson, Hewlett Packard Journal, 18, 13 (1967).

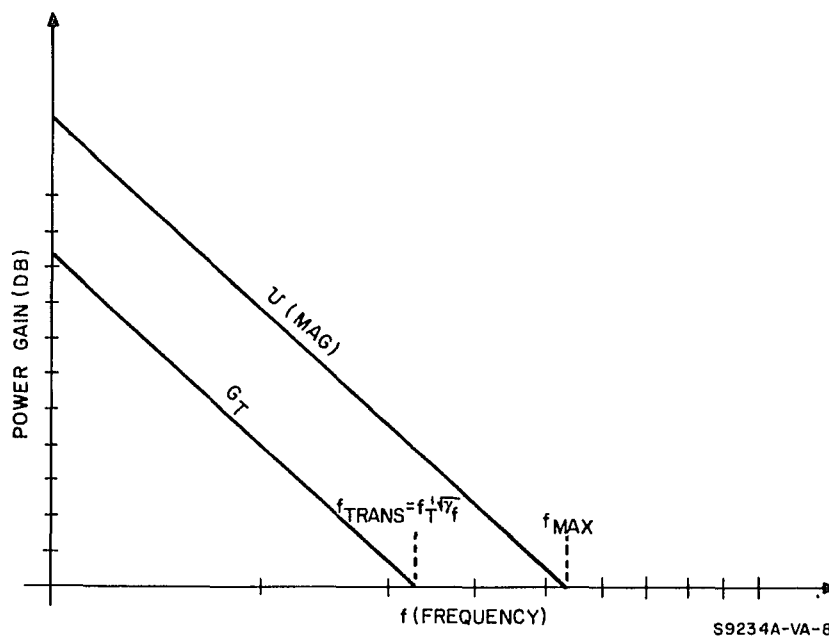


Figure 17. Transducer Power Gain,  $G_T$ , and Unilateral Maximum Power Gain,  $U(MAG)$ , Versus Frequency for a Common-Emitter Microwave Transistor

$$U(\text{MAG}) = \frac{|s_{fe}|^2}{(1 - |s_{ie}|^2)(1 - |s_{oe}|^2)} \quad (4-23)$$

Substitution of the previously derived expressions for  $s_{fe}$ ,  $s_{ie}$ , and  $s_{oe}$  into equation 4-23 yields

$$U(\text{MAG}) \doteq \left( \frac{f_{\text{MAX}}}{f} \right)^2 \quad (4-24)$$

$$f_{\text{MAX}} = \sqrt{\frac{\alpha_o f_T}{8\pi (r_b' + r_e' + r_e' + \omega_T' L_e) C_c}} \quad (4-25)$$

Equation 4-24 indicates that the  $U(\text{MAG})$  falls off at the rate of 6 dB/octave with the maximum frequency of oscillation,  $f_{\text{MAX}}$ , determined by equation 4-25. The detrimental effects of the emitter lead inductance and contact resistance are evident in equation 4-25. Figure 17 illustrates the variation of  $U(\text{MAG})$  with frequency. The  $U(\text{MAG})$  is a unique description of the microwave transistor, because it represents the forward power gain when the reverse transmission is adjusted to zero through a lossless reciprocal feedback network.<sup>4</sup> Deviations from the ideal 6 dB/octave fall-off may be attributed to the neglected second-order frequency terms in the base charging circuit time constant,  $r_b' C_c$ ; the current-gain bandwidth product,  $f_T$ ; and the input impedance,  $Z_{\text{in}}$ . If the parasitic elements associated with the emitter can be neglected,

---

<sup>4</sup>S. J. Mason, IRE Trans. on Circuit Theory, CT-1, 20, (1959).

and the transistor can be operated at high current levels, such that  $r_e$  may be neglected in equation 4-25, then the  $f_{MAX}$  becomes the familiar expression<sup>5</sup>

$$f_{MAX} = \sqrt{\frac{\alpha_o f_T}{8 \pi r_b' C_c}} \quad (4-26)$$

---

<sup>5</sup>R. L. Pritchard, Proc. IRE, 46, 1152 (1958).

transistors. The wafers, as received from Monsanto, had a special mechanical-chemical surface preparation to reduce dislocations.

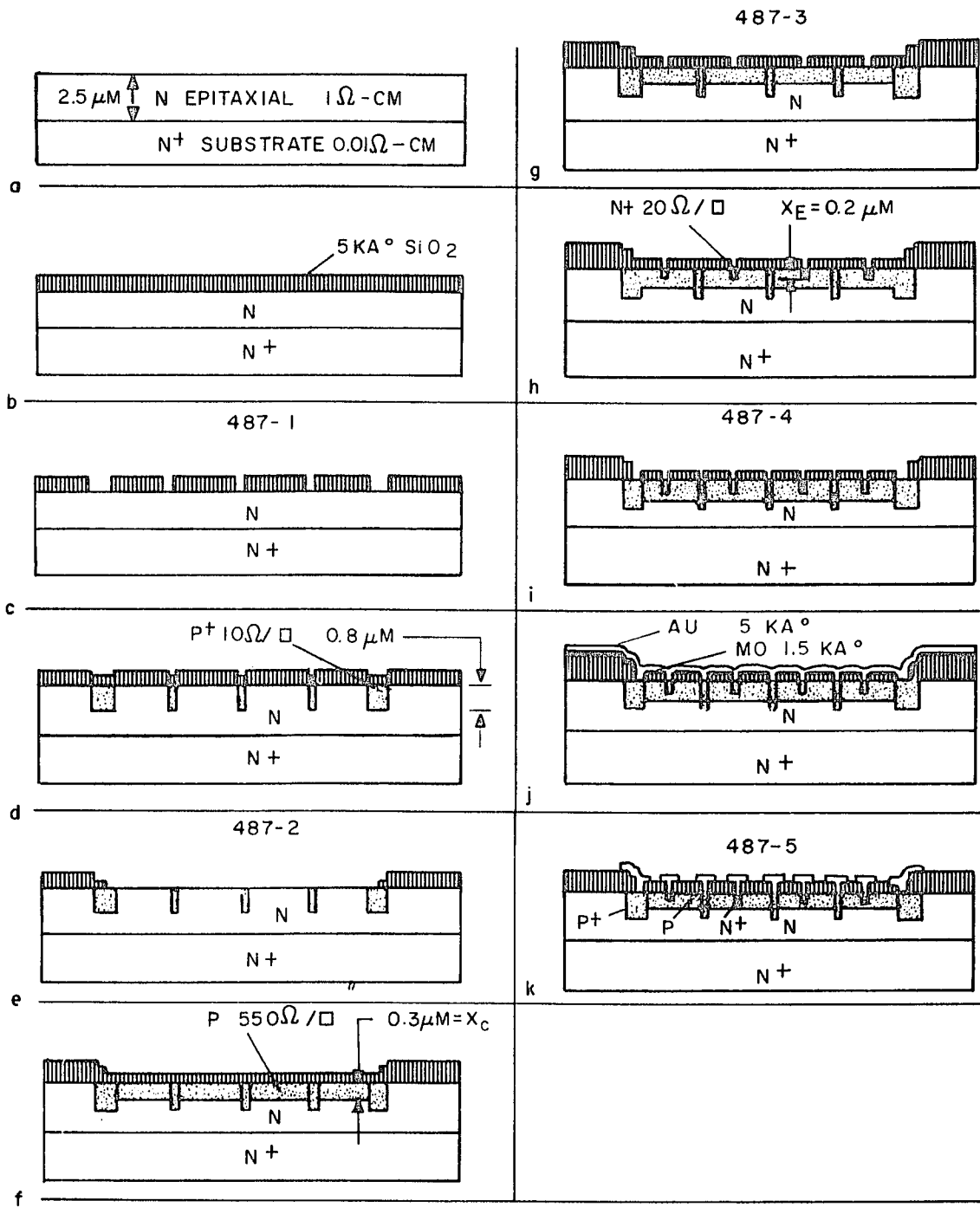
The wafers were cleaned in organic solvents and acid baths as an initial step in the processing. The organic solvents consisted of vapor-degreasing in trichloroethylene (TCE) followed by ultrasonic cleaning in acetone. The acid baths comprised the standard prediffusion cleaning method (PDC), which consisted of a fuming hot sulfuric acid bath, followed by a hot nitric acid bath, and then a final rinse in hot deionized water. Next, the wafers received a PDC, followed by oxidation to 5000 Å, with a wet-dry cycle at 1200°C. Through all of the high temperature process operations, the wafers were laid flat on the diffusion-oxidation boats to minimize the formation of dislocations due to strains induced in upright wafers.<sup>4</sup> The oxide was removed from the prepared (polished) surface of the wafer before the growth of the collector epitaxial layer. The oxide was left on the backside of the wafer to minimize the out-diffusion from the heavily doped N<sup>+</sup> substrate during the growth of the epitaxial layer.

The N-type epitaxial layer was grown with a SiCl<sub>4</sub> source vapor and a N-type AsH<sub>3</sub> dopant to a resistivity of 1 to 3 ohm-cm and a thickness of 2.5 micrometers. This operation is illustrated in Figure 18a, which

---

<sup>4</sup>P. Wang, Solid-State Technology, 12, 25 (1969).





S9446A-VB-2-1

Figure 18. Fabrication of a Silicon Microwave Transistor

will be employed to illustrate the continuous sequence of process operations. The  $N^+$  substrate received a pre-etch for 5 minutes, at  $1225^\circ\text{C}$ , with a gaseous HCl etch. The oxide was removed from the back surface of the wafer, and the wafer was subjected to a PDC operation. Next, the wafer received an oxidation to  $5000 \text{ \AA}$ , with a wet-dry cycle at  $1000^\circ\text{C}$ . This is illustrated in Figure 18b.

The first photo-engraving step (Mask #487-1, Figure 19) provided a window for the  $P^+$  base-contact and guard-ring diffusion. This is shown in Figure 18c. Figure 19 illustrates an enlargement of the Mask #487-1 (500 X), which is arranged for an overlay construction. The thin  $P^+$  grid lines were designed for 1 micrometer. The  $P^+$  base contact provided low contact resistance for the molybdenum-silicon system<sup>5</sup>, while the guard-ring prevented the premature collector-base breakdown due to junction curvature effects.<sup>6</sup> Next, the wafers received a PDC, followed by a Boron deposition at  $1000^\circ\text{C}$  and subsequent drive-in at  $1000^\circ\text{C}$ . The  $P^+$  was characterized by a sheet resistivity of 10 to 50 ohms/square and a junction depth of 0.8 to 1.0 micrometer. This corresponds to a surface concentration of  $C_o > 10^{20} \text{ atoms/cm}^3$ . The cross section of the diffusion is illustrated in Figure 18d. The Boron

---

<sup>5</sup>J. A. Cunningham, Solid-State Electronics, 8, 735 (1965).

<sup>6</sup>S. M. Sze and G. Gibbons, Solid-State Electronics, 9, 831 (1966).

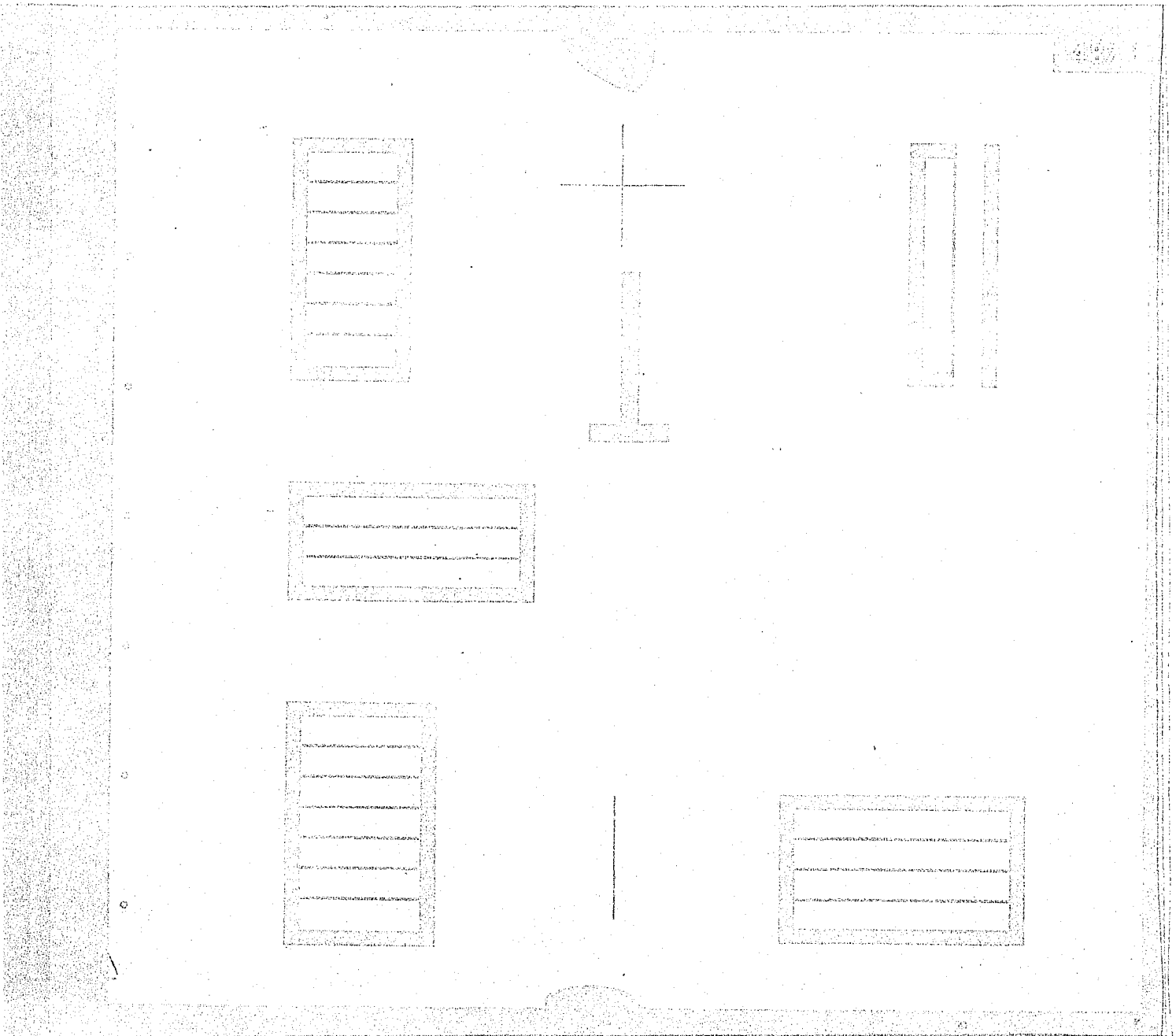
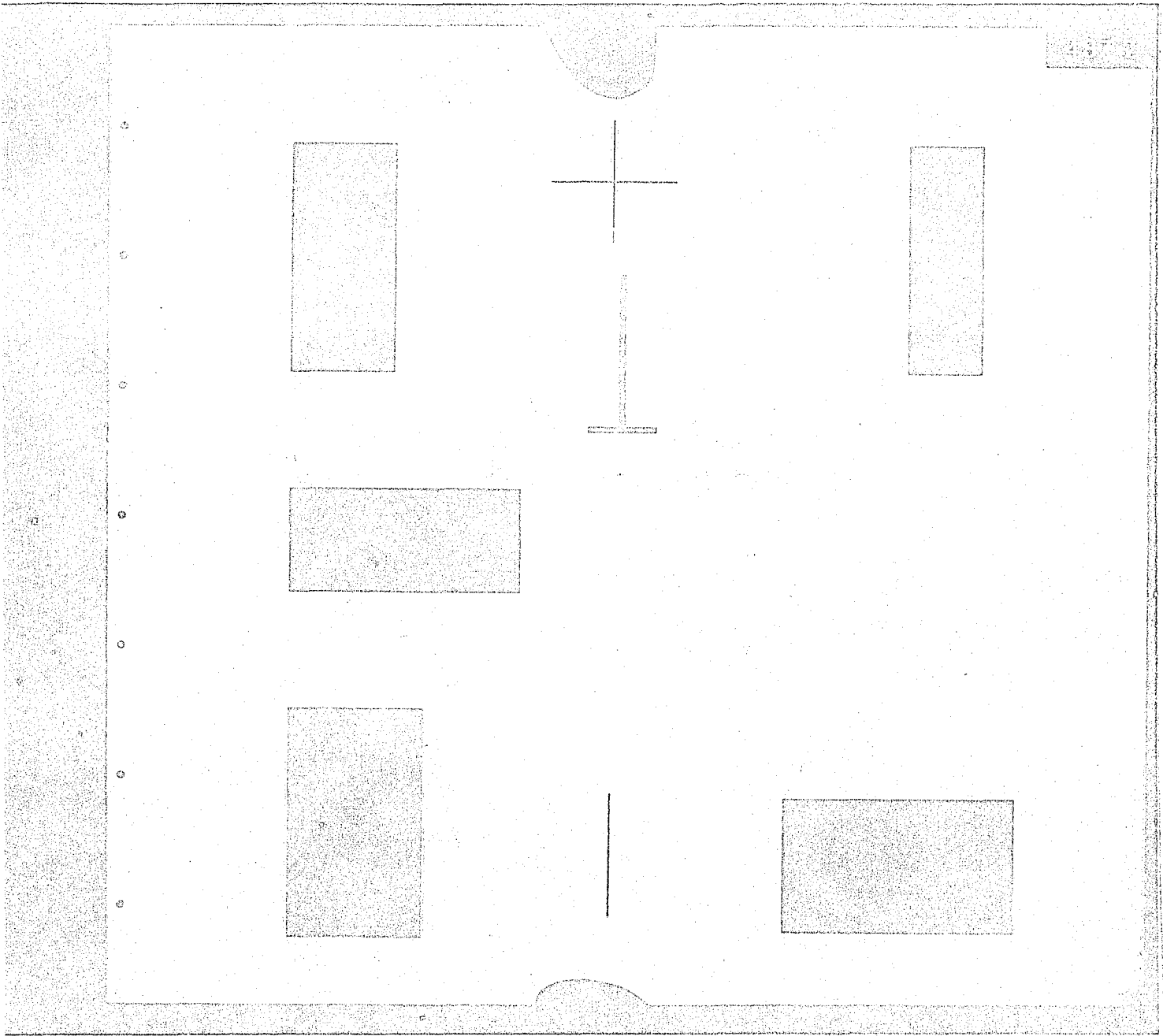
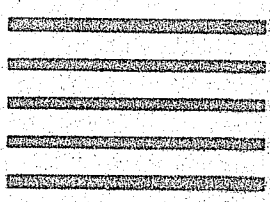
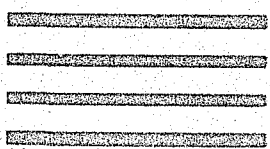
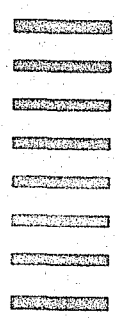
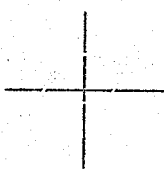


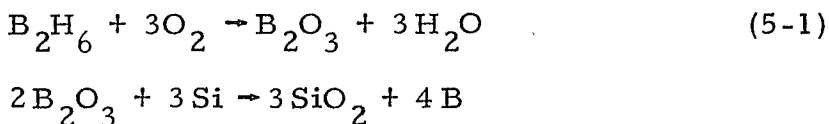
Figure 19. Photographic Masks, 487 Series, 1 Through 5 (500 X)



(11)



diffusions were performed with the gaseous impurity source,  $B_2H_6$  (diborane), and the decomposition is denoted by the reaction

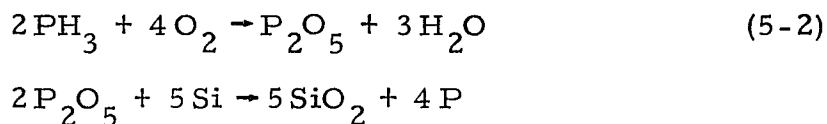


The second photo-engraving step (Mask #487-2, Figure 19) provided the window openings in the  $SiO_2$  mask for the Boron base diffusion, as shown in Figure 18e. The base deposition was performed at  $900^\circ C$ , and the drive-in was performed at  $1000^\circ C$ , to yield a base depth of 0.3 to 0.4 micrometer and a sheet resistivity of 500 to 600 ohms/square. This corresponded to a surface concentration of  $C_A \approx 2 \times 10^{19}$  atoms/cm<sup>3</sup>. The oxide regrowth during the base drive-in was approximately  $3000 \text{ \AA}$  (see Figure 18f). Figure 19 illustrates the enlargement of the Mask #487-2, and it is seen that the  $P^+$  border on Mask #487-1 overlaps the base diffusion. This was done to insure that the junction curvature effects did not limit the collector-base voltage breakdown.

The third photo-engraving step (Mask #487-3, Figure 19) provided the window openings for the phosphorus emitter diffusion, as shown in Figure 18g. The emitter mask is also shown in Figure 19. The phosphorus deposition and drive-in was a single-step process, performed at  $925^\circ C$  (see Figure 18h). This resulted in a sheet resistivity of 10 to 20 ohms/square and a base width of approximately 0.1 micrometer ( $1000 \text{ \AA}$ ). This corresponded to a surface concentration of  $C_D \approx 8 \times 10^{20}$

atoms/cm<sup>3</sup>. Figure 6 illustrates the impurity profile of the double-diffused planar epitaxial silicon microwave transistor. There were several experiments performed to minimize the base pushout, or "emitter-dip effect" (EDE), as it is commonly called.<sup>7</sup> Experiments were conducted at phosphorus deposition temperatures in the range from 900 to 950° C to determine the EDE for a constant base surface concentration of  $C_A \approx 2 \times 10^{19}$  atoms/cm<sup>3</sup>. At 925° C, the EDE was reduced in contrast to a base pushout of 0.1 micrometer at 935° C and 0.25 micrometer at 950° C. It was also observed that with the low deposition temperature of 925° C, the rate of emitter-to-collector shorts was significantly reduced in comparison to higher deposition temperatures. There is some speculation that the formation of precipitates in heavily-diffused phosphorus regions are responsible for the EDE and emitter-to-collector shorts.<sup>8</sup>

The phosphorus diffusions were performed with the gaseous impurity source, PH<sub>3</sub> (phosphine), and the decomposition is denoted by the reaction




---

<sup>7</sup>R. Gereth and G. H. Schwuttke, Appl. Phys. Letters, Jan. 1966.

<sup>8</sup>J.M. Fairfield and G.H. Schwuttke, J. Appl. Phys., 37, 1536 (1966).

In the phosphorus deposition drive-in process, a phosphorus-silicate glass of approximately  $1000 \text{ \AA}$  was deposited over the wafer and into the emitter windows. Experimentally, the phosphorus glass was found to etch at the rate of  $50 \text{ \AA/second}$  in a 1-percent HF solution. This was in contrast to the etch rate of undoped  $\text{SiO}_2$ , which is approximately  $1.25 \text{ \AA/second}$  in a 1-percent HF solution. To avoid an extremely critical alignment step for emitter contacts, the protection afforded by the lateral emitter diffusion beneath the  $\text{SiO}_2$  diffusion mask, combined with the difference between the above etch rates, was employed in the fabrication process. After the emitter diffusion, the phosphorus-silicate glass was removed with the selective etch<sup>9</sup>, while maintaining the oxide protection over the emitter junction. The lateral diffusion beneath the  $\text{SiO}_2$  was not affected by the size of the emitter window, since the width of the window,  $h > 8(Dt)^{1/2}$ , where,  $D$  is the diffusion constant of phosphorus at  $925^\circ \text{ C}$  and  $t$  is the time.<sup>10</sup> The slight difference between the lateral and downward diffusions could be attributed to the gradient in the base concentration from the surface into the bulk.

---

<sup>9</sup> emitter dip etch with 1-percent HF etchant.

<sup>10</sup> D.P. Kennedy and P.C. Murley, IBM J. Res. and Dev., 10, 6 (1966). In the experiments performed,  $(Dt)^{1/2} \approx 0.02$  micrometer, while the window opening,  $h > 1$  micrometer.



The next photographic step was Mask #487-4 (see Figure 19), which provided the window openings for the base contact metallization (see Figure 18i). After the oxide was etched, the wafer received a molybdenum-gold metallization (see Figure 18j). The molybdenum was dc sputtered to a thickness of  $1500 \text{ \AA}$  ( $< 1 \text{ ohm/square}$ ), followed by a gold sputtering of  $5000 \text{ \AA}$  ( $0.1 \text{ ohm/square}$ ). The molybdenum functions as a diffusion barrier to prevent the formation of a gold-silicon eutectic at the bonding temperature, and it also provides adherence to the  $\text{SiO}_2$ . This particular metallization was selected after an evaluation of the conventional aluminum metallization showed the presence of emitter-to-base shorts in shallow-diffused microwave transistors. The emitter-to-base shorts were tracked to diffusion migration of aluminum, along the Si-SiO<sub>2</sub> interface, at and above the bonding temperature ( $385^\circ \text{ C}$ ). The migration of aluminum by diffusion along the boundary is believed to be a vacancy-enhanced mechanism associated with the stress at the Si-SiO<sub>2</sub> interface. Experiments were performed to illustrate that temperatures greater than  $400^\circ \text{ C}$  and sintering times of 5 to 15 minutes resulted in aluminum migration distances of greater than  $5000 \text{ \AA}$ . In an attempt to restrict the migration, the temperature was lowered to the  $390\text{-to-}400^\circ \text{ C}$  range; however, when emitter junction depths of less than  $5000 \text{ \AA}$  were employed, the aluminum migration resulted in emitter-to-base shorts. Thus, it was

apparent that a metallization procedure was needed to alleviate this diffusion migration problem. The last photo-engraving step was the interconnection mask (Mask #487-5, Figure 19) which is shown in Figure 18k. The gold was etched in a dilute KI and iodine etchant, while the molybdenum was etched in a  $\text{H}_3\text{PO}_4$  -  $\text{HNO}_3$  etchant. Ohmic contacts were obtained by sintering the devices, in the temperature range from 390 to 410° C for 5 to 15 minutes, in a nitrogen atmosphere. Figure 20 illustrates a completed version of the microwave transistor.

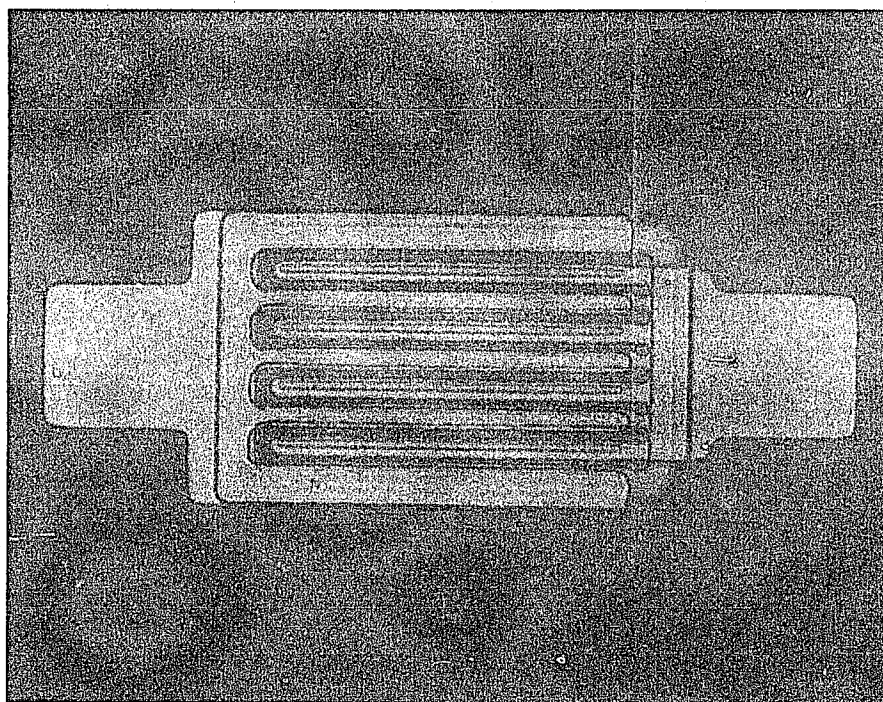


Figure 20. Silicon Microwave Transistor

## CHAPTER VI

### EXPERIMENTAL RESULTS

#### 6.1 Microwave Measurements

The microwave transistors were evaluated in the test fixture shown in Figure 21. This fixture holds a 1.0 x 1.0 x 0.025-inch alumina substrate ( $\text{Al}_2\text{O}_3$ ), which has a relative dielectric constant  $K_d \doteq 9$ . The alumina substrate is used in a microstrip line configuration that consists of a strip conductor parallel to a ground plane, as shown in Figure 22. The microstrip transmission line offers a convenient method for coupling microwave energy to various positions in a microwave hybrid integrated circuit. The alumina substrate has a ground plane and microstrip transmission lines formed through a chrome-gold evaporation of 20  $\overset{\circ}{\text{k}}\text{Å}$  followed by gold plating to 0.4 mil. Since it is a mixed dielectric system, it cannot support a pure TEM mode; however, a quasi-TEM mode approximation has been employed to describe the properties of the line.<sup>1</sup> The fringing fields are confined to the region of the strip line conductor by the high dielectric constant substrate.

---

<sup>1</sup>H.A. Wheeler, IEEE Trans. Microwave Theory and Techniques, MTT-12, 280 (1964)

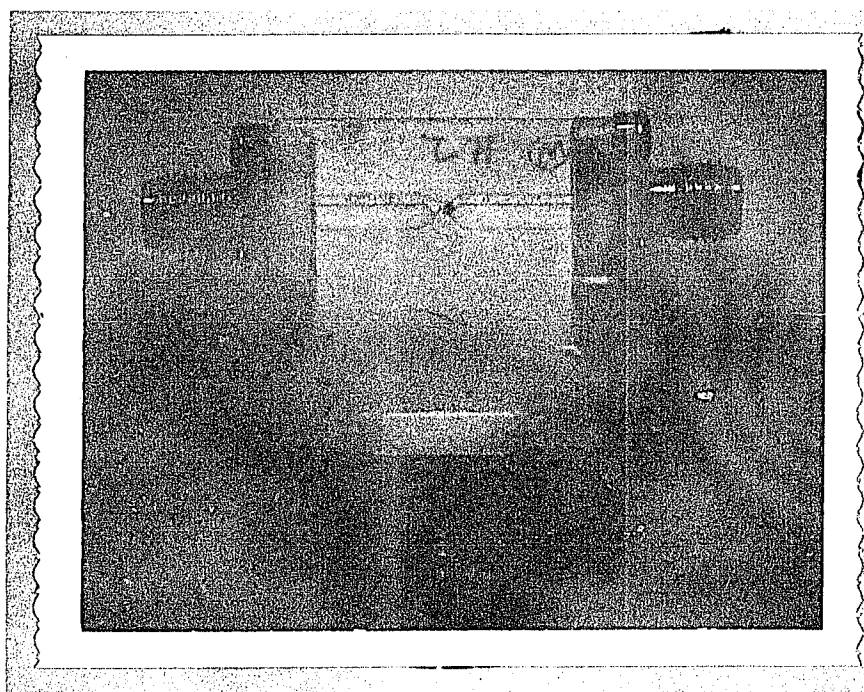
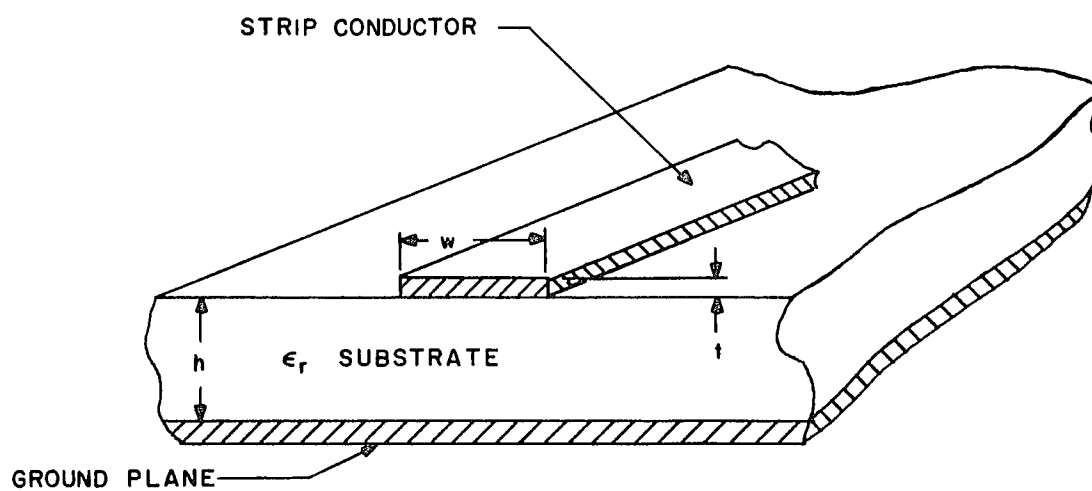


Figure 21. Microwave Transistor Test Fixture



$$Z_0 = \frac{377}{\sqrt{\epsilon_r}} \left( \frac{h}{W'} \right) \frac{1}{1 + 1.735 \epsilon_r^{-0.0724} \left( \frac{W'}{h} \right)^{-0.836}} \text{ OHMS}$$

S8528A - VA - 5

$$W' = W + \frac{t}{\pi} \left( 1 + \ln \frac{2h}{t} \right)$$

Figure 22. Microwave Transmission Line Geometry

Design data is available for the microstrip line<sup>2, 3</sup>, and the width of the line was chosen as 0.025 inch to provide a characteristic impedance of  $Z_o = 50$  ohms.

The collector (substrate) of the microwave transistor was eutectically bonded to the output microstrip line, while the base of the transistor was wire-bonded to the input microstrip line. The emitter of the transistor was wire-bonded to a large bypass capacitor that used the alumina as the dielectric. The bonding wire was an 0.8-mil diameter gold wire, and the length varied from 10 to 20 mils. The test fixture employed OSM pressure connectors to contact the microstrip lines and provide transitions to 7 mm type connectors. The electrical diagram of the RF and biasing circuits is shown in Figure 23 in which the emitter resistor,  $R_E$ , provides operating point and signal stability. Biasing Tee's were used for the input and output circuits, as indicated in Figure 23.

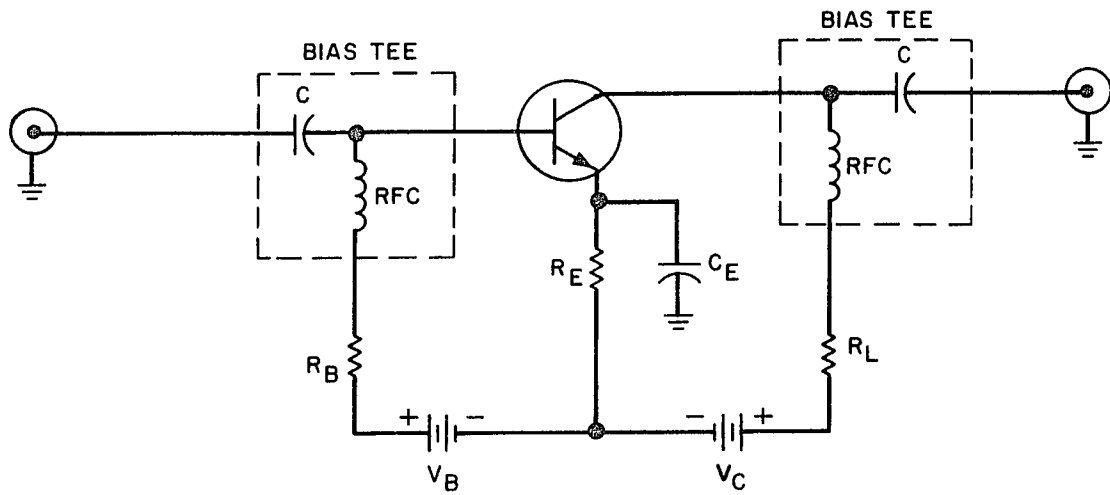
The measurements were performed on a Hewlett-Packard 8410A Network Analyzer System.<sup>4</sup> The insertion gains were determined with the experimental set-up shown in the block diagram of Figure 24. The transmission system was calibrated with a 1.0 x 1.0 x 0.025-inch

---

<sup>2</sup>H.A. Wheeler, IEEE Trans. Microwave Theory and Techniques, MTT-13, 172 (1965).

<sup>3</sup>M. Caulton, et. al, RCA Review, 27, 377 (1966).

<sup>4</sup>R.W. Anderson, Hewlett Packard J., 18, 13 (1967).



S9234A-VA-6

Figure 23. Electrical Circuit Diagram of RF and Biasing for the Microwave Transistor



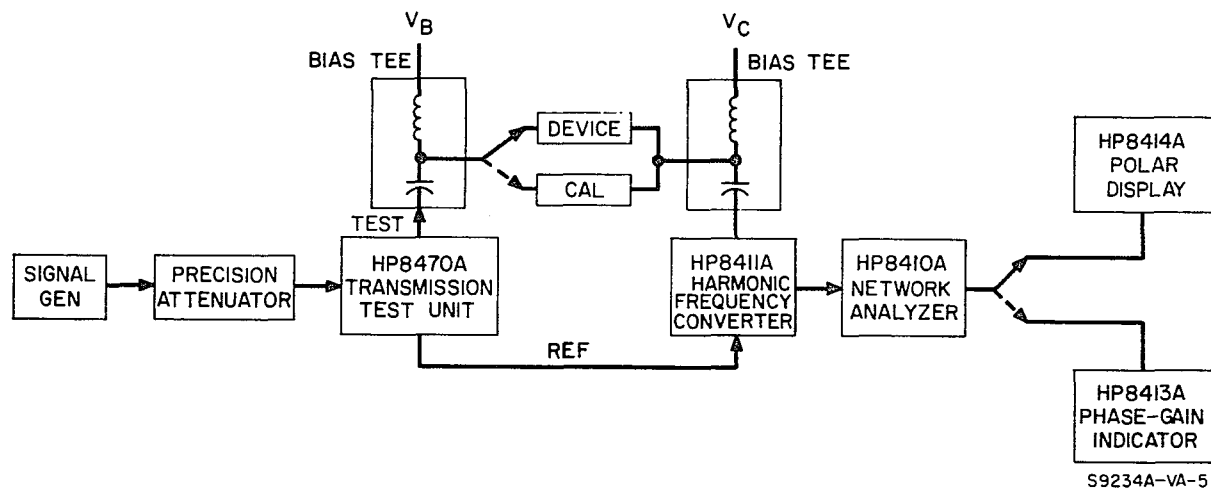


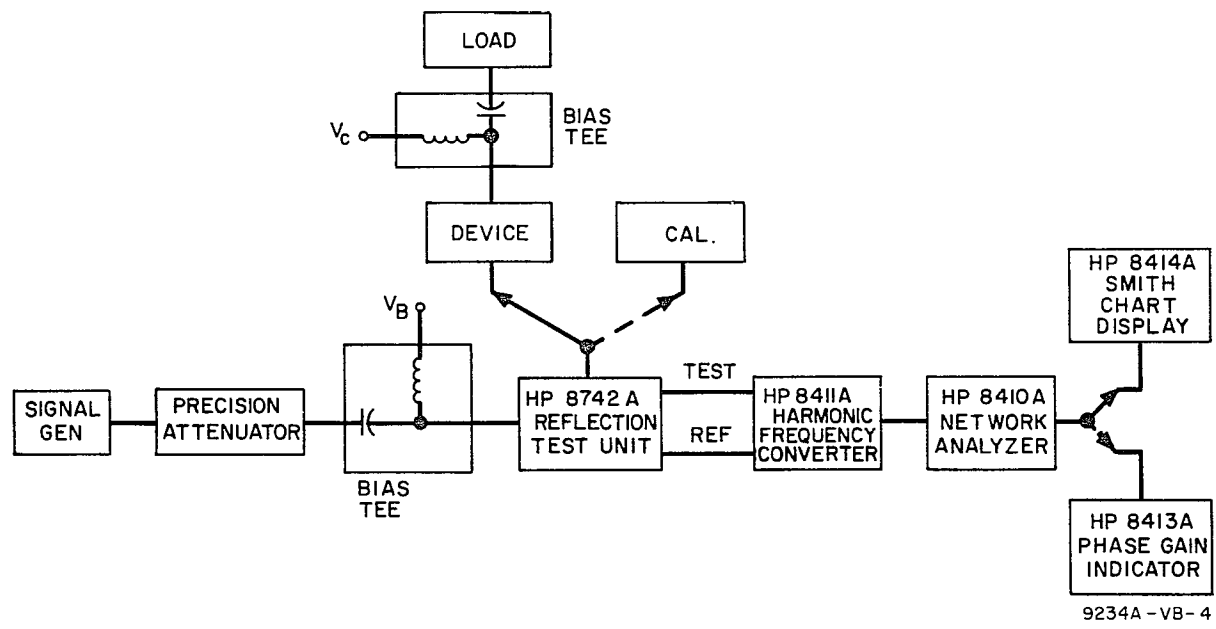
Figure 24. Block Diagram  $S_{21}$  and  $S_{12}$  (Measurement of Transmission Parameters)

straight-feed microstrip transmission line. The reflection measurements were with the experimental set-up shown in Figure 25. The reflection system was calibrated with a 1.0 x 0.5 x 0.025-inch straight-feed microstrip transmission line that was shorted at the end. The phase equalization in the transmission and reflection measurements was provided by a variable line stretcher. The measurements included the effects of the bonding wire lead inductance.

Figure 26 illustrates the s-parameters measured on an experimental microwave transistor in the common-emitter configuration. The parameters were measured in the frequency range from 1.0 through 6.0 GHz and included the effects of the bonding wire inductance in the base and emitter legs of the transistor. Figure 27 illustrates the transducer gain,  $G_T = |s_{fe}|^2$  and the maximum unilateral power gain U(MAG), which were discussed in paragraph 4.3.

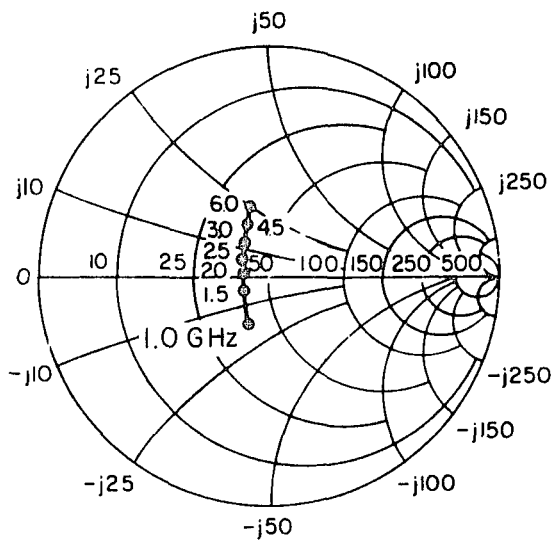
## 6.2 Device Test Structure

The device test structure employed in the determination of the sub-surface sheet resistance and associated elements in the base-charging circuit (paragraph 3.2) is shown in Figure 19, with the 3 bonding pads. Figure 28 illustrates the equivalent circuit of this test structure with the various elements of the base-charging circuit time constant  $r_b' C_c$ . The emitter and collector of the test structure are shorted at the ends of the emitter in order to avoid sneak leakage paths between base

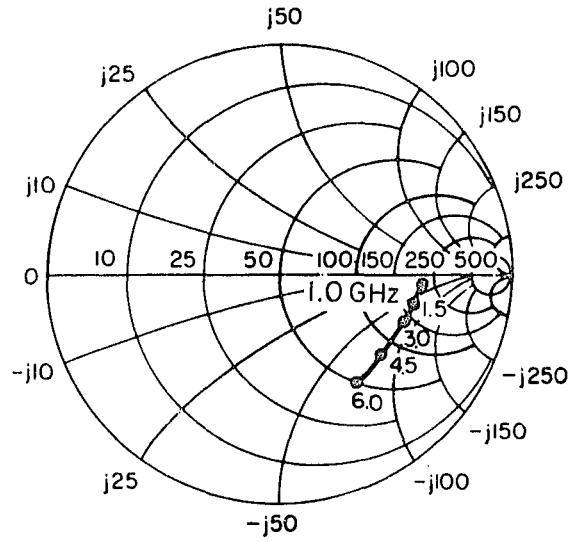


9234A - VB - 4

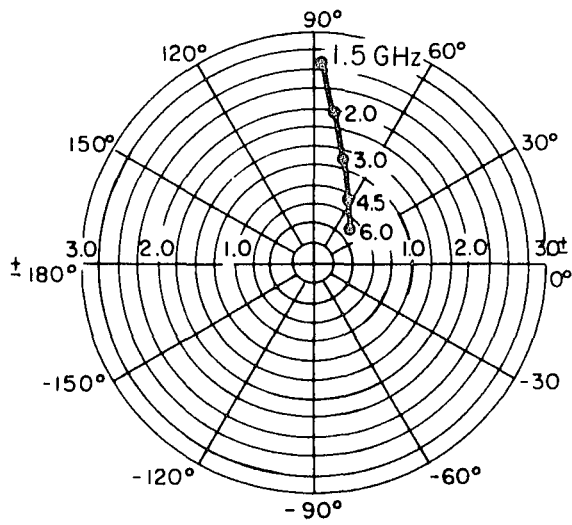
Figure 25. Block Diagram  $S_{11}$  and  $S_{22}$  (Measurement of Reflection Parameters)



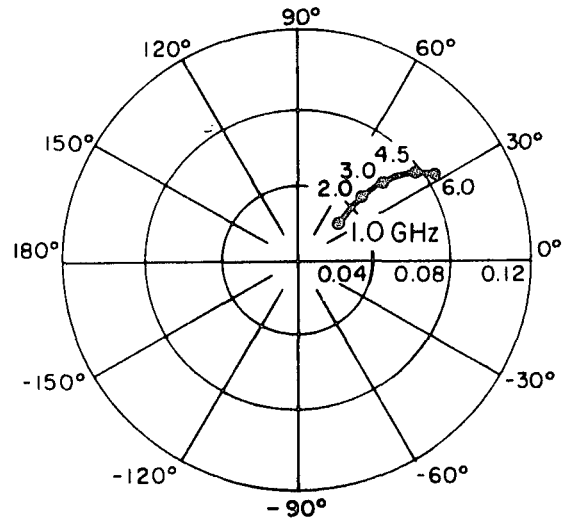
COORDINATES IN OHMS  
 A. INPUT IMPEDANCE AND INPUT REFLECTION COEFFICIENT,  $S_{11e}$



COORDINATES IN OHMS  
 B. OUTPUT IMPEDANCE AND OUTPUT REFLECTION COEFFICIENT,  $S_{22e}$



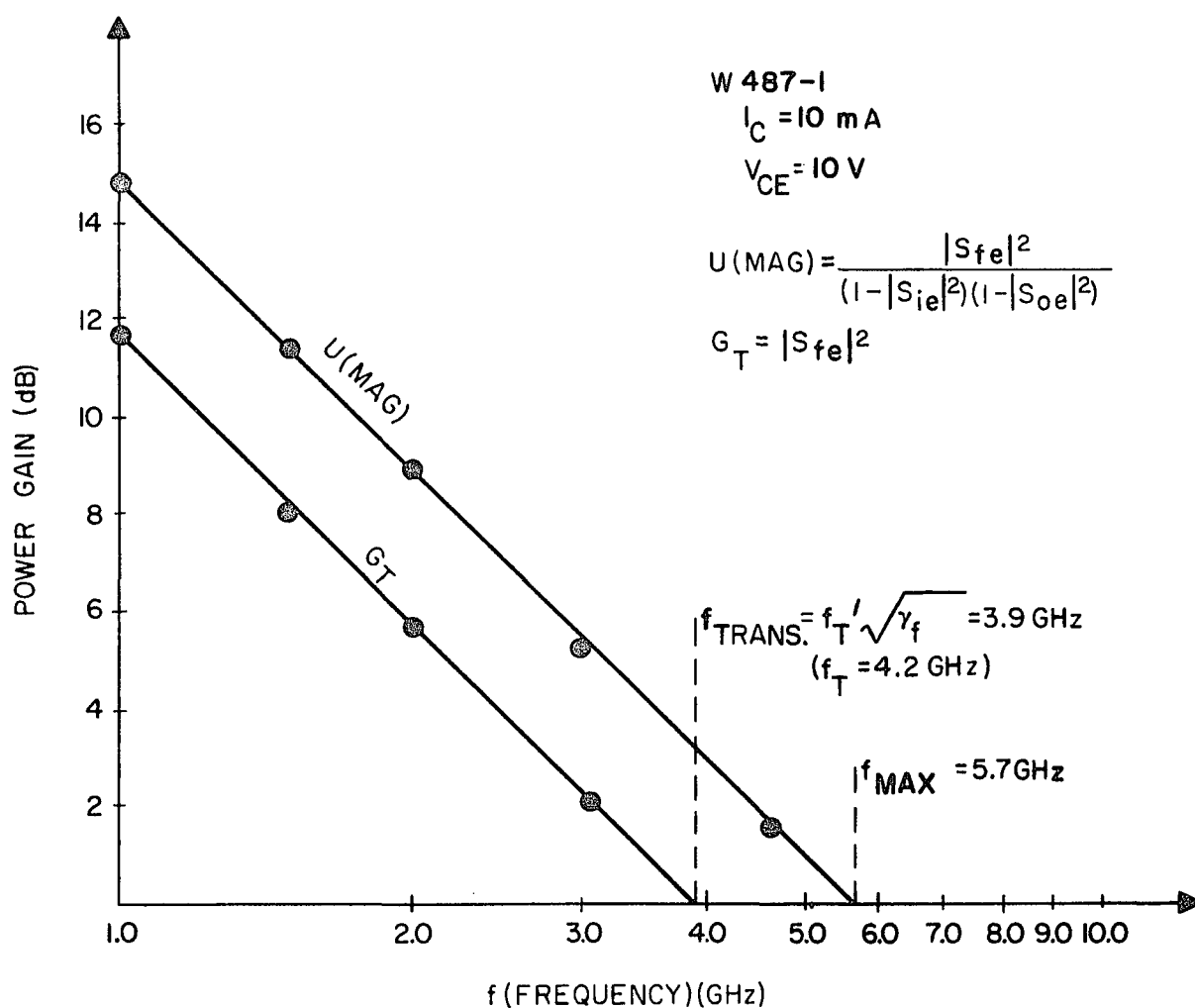
C. FORWARD TRANSFER COEFFICIENT,  $S_{21e}$



D. REVERSE TRANSFER COEFFICIENT,  $S_{12e}$

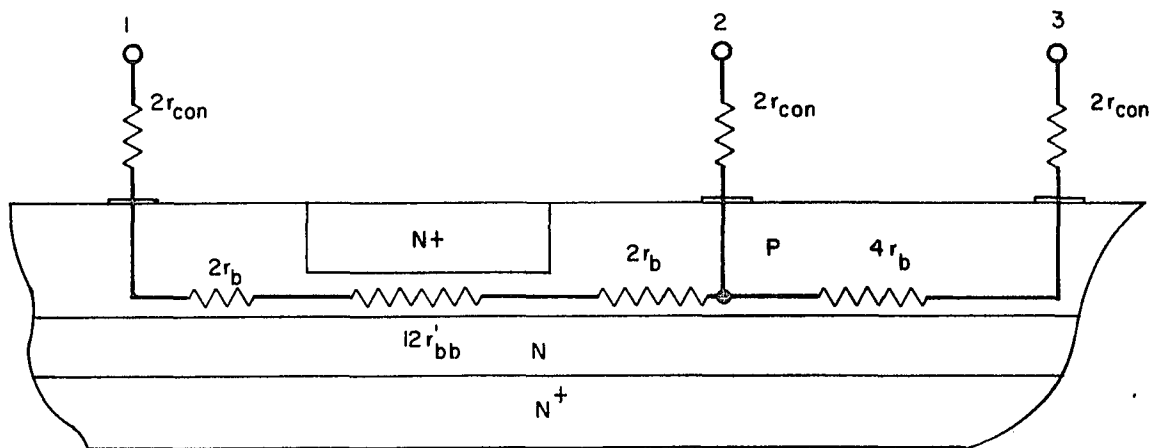
9687A-BA-3

Figure 26. S-Parameters for an Experimental Silicon Microwave Transistor in the Frequency Range from 1.0 to 6.0 GHz ( $I_c = 10$  mA,  $V_c = 10$  V)



S9234A-VA-2-1

Figure 27. Transducer Power Gain,  $G_T$  (lower curve) and Unilateral Power Gain,  $U(\text{MAG})$  (upper curve) for a Silicon Microwave Transistor



S9446A-VA-4

Figure 28. Device Test Structure to Determine Elements of the Base-Charging Circuit Time Constant,  $r'_b C_c$

terminals. A measurement of the 3 resistances:  $R_{12}$ ,  $R_{13}$  and  $R_{23}$  enable the components of the base charging circuit to be determined.

Examination of the equivalent circuit of Figure 28 shows,

$$\begin{aligned} r'_{bb} &= \frac{R_{13} - R_{23}}{12} \text{ per emitter strip} \\ r_b &= \frac{R_{13} - R_{12}}{4} \text{ per emitter strip} \\ r_{con} &= \frac{R_{12} + R_{23} - R_{13}}{4} \text{ per emitter strip} \end{aligned} \quad (6-1)$$

### 6.3 Transistor Equivalent Circuit Parameters

In this paragraph, the small-signal equivalent circuit parameters shown in Figure 13 will be calculated for the microwave transistor geometry illustrated in Figures 19 and 20.

#### a. List of Constants:

Electronic charge:  $q = 1.6 \times 10^{-19} \text{ C}$

Permittivity of free space:  $\epsilon_o = 8.85 \times 10^{-14} \text{ F/cm}$

Boltzmann's constant:  $k_B = 8.63 \times 10^{-5} \text{ eV/}^\circ\text{K}$

Dielectric constant of Si:  $K_s = 12$

Dielectric constant of  $\text{SiO}_2$ :  $K_o = 4$

#### b. Emitter-Base Junction:

$C_N$  = neutral capacitance, calculated from Figure 10, with

impurity gradient,  $a_I = 1 \times 10^{23} \text{ cm}^{-4}$

= 7.6 pF

$$C_s = \text{space-charge capacitance, calculated from Figure 10,} \\ \text{with impurity gradient, } a_I = 1 \times 10^{23} \text{ cm}^{-4} \\ = 0.06 \text{ pF}$$

$$C_T = \text{total capacitance associated with the transition region} \\ \text{of the emitter-base junction} \\ = C_N + C_S = 7.66 \text{ pF}$$

$$r_e = \text{incremental forward resistance of the forward biased} \\ \text{emitter-base junction}$$

$$= \frac{k_B T}{q I_E} = 2.6 \text{ ohms}$$

$$r_e^i = \text{emitter contact resistance (dc measurement)} \\ = 1.2 \text{ ohms}$$

$$I_E = 10 \text{ mA; } V_{CE} = 10 \text{ V; } V_{EB} = 0.76 \text{ V}$$

$$A_E = \text{junction area} \doteq 5.0 \times 10^{-6} \text{ cm}^2$$

$$\ell = \text{length of diffused emitter strip} = 6.2 \times 10^{-3} \text{ cm}$$

$$h = \text{width of diffused emitter strip} = 2 \times 10^{-4} \text{ cm}$$

$$d = \text{distance between emitter-base strips} = 5 \times 10^{-4} \text{ cm}$$

$$n = \text{number of emitter strips} = 4$$

c. Collector-Base Junction:

$$x = \text{depletion layer width, calculated from Lawrence}$$

$$\text{Warner curves with } C_o/C_B = 10^{-4} \text{ (} C_B = 3 \times 10^{15} \text{ cm}^{-3}\text{)} \\ = 1.5 \times 10^{-4} \text{ cm}$$



$$\begin{aligned}
 C_a &= \text{capacitance per unit area, calculated from Lawrence} \\
 &\quad \text{Warner curves with } C_o/C_B = 10^{-4} \text{ (} C_B = 3 \times 10^{-5} \text{ cm}^{-3}\text{)} \\
 &= 8.5 \times 10^3 \text{ pF/cm}^2
 \end{aligned}$$

$$C_{BP} = \text{capacitance per unit area of bonding pad}$$

$$= \frac{K_o \epsilon_o}{t_{ox}} = 7.1 \times 10^3 \text{ pF/cm}^2$$

$$C_i = \text{depletion layer capacitance under emitter strips}$$

$$= nh\ell C_a = 0.04 \text{ pF}$$

$$C_b = \text{depletion layer capacitance between emitter and base strips}$$

$$= n(2d)\ell C_a = 0.20 \text{ pF}$$

$$C_A = \text{depletion-layer capacitance other than } C_i \text{ and } C_b, \text{ plus bonding pad capacitance, } C_{BP}$$

$$= C_a A_{CB} - C_i - C_b + \frac{K_o \epsilon_o}{t_{ox}} A_{BP}$$

$$= 0.33 - 0.04 - 0.20 + 0.05$$

$$= 0.14 \text{ pF}$$

$$r_c = \text{collector junction resistance (dc measurement), which is not shown in Figure 13}$$

$$= 5,000 \text{ ohms}$$

$$V_{CB} = \text{collector-base bias voltage} = 9.25 \text{ V}$$

$$N_D = \text{epitaxial layer doping} = 3 \times 10^{15} \text{ cm}^{-3}$$

$A_{CB}$  = area of collector-base junction (2 mils x 3 mils)

$A_{BP}$  = area of bonding pad (1 mil x 1 mil)

$t_{ox}$  = oxide thickness under bonding pad = 5 k Å

d. Base-Charging Circuit:

$r'_{bb}$  ( $m_o = 0$ ) = transverse base resistance, with zero carrier injection and  $V_{CB} = 0$  (dc measurement)  
= 19.5 ohms

$r_b$  = interstrip base resistance (dc measurement)  
= 4.8 ohms

$r_{con}$  = contact resistance (dc measurement)  
= 3.6 ohms

$m_o$  = modulation level

$$m_o = \frac{I_E W k}{q A_E \bar{D}_n N_A(0)} = \frac{10 \times 10^{-3} \times 1.2 \times 10^{-5} \times 0.33}{1.6 \times 10^{-19} \times 5.0 \times 10^{-6} \times 8 \times 5 \times 10^{16}} \doteq 0.12$$

$W$  = electrical base width =  $1.2 \times 10^{-5}$  cm.

$k$  =  $\bar{N}_A / N_A(0) = 0.33$

$\bar{D}_n$  = average diffusion constant (electrons) =  $8 \text{ cm}^2/\text{sec}$

$N_A(0)$  = base doping density at edge of depletion layer  
=  $5 \times 10^{16} \text{ cm}^{-3}$

$$\begin{aligned}
 r'_{bb}(m_o=0.12) &= \text{modulated transverse base resistance} \\
 &= 0.8 r'_{bb}(m_o=0) \\
 &= 15.6 \text{ ohms (calculated from equation 2-36)}
 \end{aligned}$$

$$\begin{aligned}
 r'_b &= \text{total base resistance} \\
 &= r'_{bb}(m_o) + r_b + r_{con} \\
 &= 15.6 + 4.8 + 3.6 = 24.0 \text{ ohms}
 \end{aligned}$$

$$\begin{aligned}
 r'_b C_c &= \text{base charging circuit time constant} \\
 &= r_{con} (C_i + C_b + C_A) + (r_b + r'_{bb}) C_i + r_b C_b \\
 &= 3.6 (0.38) + 20.4 (0.04) + 4.8 (0.20) \\
 &= 1.37 \text{ psec} + 0.82 \text{ psec} + 0.96 \text{ psec} \\
 &= 3.15 \text{ psec}
 \end{aligned}$$

$$\begin{aligned}
 C_c &= \text{effective capacitance in equivalent circuit} \\
 &= 0.13 \text{ pF}
 \end{aligned}$$

$$\begin{aligned}
 r_s &= \text{collector series resistance (dc measurement)} \\
 &= 25 \text{ ohms}
 \end{aligned}$$

e.  $f_T$  and  $f_{MAX}$  Calculation:

$$T_{EC} = \frac{W^2}{\lambda D_n} + \frac{x}{2V_L} + r_e (C_T + C_c) + (r_s + r'_e) C_c$$

(base transit time + collector depletion layer transit time) + (emitter time constant) + (collector time constant)

$$= \tau_b + \tau_d + \tau_e + \tau_c$$

= total emitter-to-collector transit time

$$= 5.0 \text{ psec} + 8.5 \text{ psec} + 20.2 \text{ psec} + 3.4 \text{ psec}$$

$$= 37.1 \text{ psec}$$

$$\tau_b = \frac{1 + \alpha_o m}{\alpha_o \omega \alpha} = \frac{W^2}{\lambda \bar{D}_n} = \frac{(0.12 \times 10^{-4})^2}{3.5 \times 8} = 5.0 \text{ psec}$$

$$\alpha_o = \text{low frequency current gain} = 0.99$$

$$m = \text{excess phase shift} = 0.4 \text{ radians}$$

$$\tau_d = \frac{x}{2V_L} = \frac{1.5 \times 10^{-4}}{2 \times 8.8 \times 10^6} = 8.5 \text{ psec}$$

$$V_L = \text{maximum scatter-limited velocity of electrons in silicon} = 8.8 \times 10^6 \text{ cm/sec}$$

$$\tau_e = r_e (C_T + C_C) = 2.6 (7.66 + 0.13) = 20.2 \text{ psec}$$

$$\tau_c = (r_s + r'_e) C_C = (25 + 1.2) (0.13) = 3.4 \text{ psec}$$

$$f_T = \frac{1}{2\pi \tau_{ec}} = \frac{1 \times 10^{12}}{2\pi (37.1)} = 4.2 \times 10^9 \text{ (4.2 GHz)}$$

$$f'_T = \frac{f_T}{1 + \omega_T C_c Z_o} = \frac{4.2 \times 10^9}{1 + 2\pi (4.2 \times 10^9)(0.13 \times 10^{-12})(50)}$$

$$= 3.6 \times 10^9 \text{ (3.6 GHz)}$$

$$L_b = \text{base lead inductance} = 0.16 \text{ nH} \quad (\text{RF measurement})$$

$$L_e = \text{emitter lead inductance} = 0.45 \text{ nH}$$

$$f_{\text{MAX}} = \sqrt{\frac{\alpha_o f_T}{8\pi (r'_b + r'_e + r_e + \omega'_T L_e) C_c}}$$

Substitution of the device parameters into the above expression yields,

$$f_{\text{MAX}} \doteq 5.8 \times 10^9 \text{ (5.8 GHz)}$$

## CHAPTER VII

### CONCLUSIONS

As a result of the studies and experiments performed in this thesis, the following conclusions can be drawn:

a. The lumped small-signal T-equivalent circuit for the microwave transistor provides an adequate model to explain the frequency variation of s-(scattering) parameters. The input and output of the microwave transistor may be characterized by a series RLC and parallel  $R_o C_o$  equivalent circuit, respectively. This was substantiated by s-parameter measurements in the frequency range from 1.0 to 6.0 GHz on silicon transistors with an  $f_T > 4$  GHz and  $f_{MAX} > 6$  GHz.

b. The design of a microwave transistor small-signal amplifier requires a high collector resistivity (e.g., 1 to 3 ohm-cm); compatible with current density limitations. The design also requires a shallow diffusion profile (e.g.,  $x_E = 0.2$  micrometer and  $x_C = 0.3$  micrometer) to minimize the product of the subsurface sheet resistance,  $R_{ss}$ , and the base-collector capacitance/area,  $C_a$ . Shallow diffusion profiles provide steep impurity gradients at the emitter and

collector junctions. These gradients reduce the neutral capacitance of the emitter-base junction and the base-widening of the collector junction. These results were concluded from numerical calculations on the computer and verified with experimental silicon microwave transistors.

c. The fabrication of silicon microwave transistors requires uniform, thin, photoresist to print the 1-micrometer emitter strips. Low temperature emitter diffusions are required to minimize the base push-out or emitter dip-effect (EDE). A (100) orientation for the silicon substrates is desired to reduce the emitter-to-collector shorts incurred during fabrication. An emitter dip etch is used to avoid a difficult alignment of the contact metallization mask for the emitter strips. Finally, the molybdenum-gold metallization system is employed to replace the conventional aluminum contact metallization. The aluminum metallization resulted in a large number of emitter-to-base shorts, which were caused by aluminum migration along the Si-SiO<sub>2</sub> interface at low temperatures.

d. As a result of the investigations performed in this thesis, it is concluded that the microwave performance of the transistor as an amplifier is limited by the base contact resistance and the emitter lead inductance. The development of techniques to minimize the contact

resistance, such as high surface concentration diffusions and surface preparation of the semiconductor, are important to increase the  $f_{MAX}$  of the transistor. The emitter lead inductance may be reduced by the use of beam-lead technology. It is anticipated that through these developments, the silicon microwave transistor will provide direct signal amplification in the X-band microwave region.



## BIBLIOGRAPHY

- Abraham, R. P. IRE Transactions on Electron Devices, ED-7, (1960), 59.
- Anderson, R. W. Hewlett-Packard Journal, 18, (1967), 13.
- Bardeen, J. and Brattain, W. Physical Review, 74, (1948), 230.
- Beadle, W. E., et al. IEEE Transactions on Electron Devices, ED-16, (1969), 125.
- Boltaks, B. I. Diffusion in Semiconductors. New York: Academic Press, 1963.
- Bradley, W. E. Proceedings IRE, 41, (1953), 1702.
- Caulton, M., et al. RCA Review, 27, (1966), 377.
- Cunningham, J. A. Solid-State Electronics, 8, (1965), 735.
- Dhaka, V. A. IBM Journal of Research and Development, 12 (1968), 476.
- Early, J. M. Bell Systems Technical Journal, 32 (1953), 1271.
- Early, J. M. Bell Systems Technical Journal, 33 (1954), 517.
- Early, J. M. Proceedings IRE, 40, (1952), 1401.
- Early, J. M. Proceedings IRE, 46, (1958), 1177.
- Edwards, R. and Prichett, R. L. NEREM Record. Boston, Mass., 1965.
- Fairfield, J. M. and Schwuttke, G. H. Journal of the Electrochemical Society, 115 (1968), 415.
- Fairfield, J. M. and Schwuttke, G. H. Journal of Applied Physics, 37 (1966), 1536.
- Gereth, R. and Schwuttke, G. H. Applied Physics Letters, Jan., 1966.

- Ghosh, H. W., et al. Solid-State Electronics, 10, (1967), 705.
- Giacoletto, L. J. RCA Review, 15, (1954), 506.
- Hannay, N. B., ed. Semiconductors. New York: Rheinhold, 1960.
- Hoerni, J. A. IRE Transactions on Electron Devices, ED-8, (1961), 178.
- Irvin, J. C. Bell Systems Technical Journal, 41 (1962), 391.
- Johnson, G. Solid-State Communications. Edited by J. R. Miller, New York: McGraw-Hill, 1966.
- Kennedy, D. P. Final Report Number 1. Report to the United States Air Force, April 1, 1966, contract number AF19(628)-5072.
- Kennedy, D. P. and Murley, D. C. IBM Journal of Research and Development, 10 (1966), 6.
- Keonjian, E. Microelectronics. New York: McGraw-Hill, (1963).
- Kirk, C. T., Jr. IRE Transactions on Electron Devices, ED-9, (1962), 164.
- Kroemer, H. Arch. Elekt Übertragung, 8, (1954); 223, 363, 449.
- Kurokawa, K. IEEE Transactions on Microwave Theory and Techniques. MTT-13, 1965, 194.
- Law, R. R., et al. Proceedings IRE, 40, 1952, 1352.
- Lawrence, H. and Warner, R. Bell Systems Technical Journal, 39 (1960), 389.
- Lee, C. A. Bell Systems Technical Journal, 35 (1956), 23.
- Linville, J. G. and Gibbons, J. F. Transistors and Active Circuits. New York: McGraw-Hill, 1961.
- Lloyd, R. IRE Transactions on Electron Devices, ED-13, (1966), 991.
- McLouski, R. M. NASA Contractor Report. Report number NASA CR-597 to the National Aeronautics and Space Administration, 1966.
- Mason, S. J. IRE Transactions on Circuit Theory, CT-1, (1959), 20.

- Morgan, S. P. and Smits, F. M. Bell Systems Technical Journal, 39 (1960), 1573.
- O'Grady, R. P. Microelectronics and Reliability, 7, (1968), 233.
- Pritchard, R. L. Proceedings IRE, 40, (1952), 1476.
- Pritchard, R. L. Proceedings IRE, 46, (1958), 1152.
- Rittmann, A. D., et al. IRE Transactions on Electron Devices, ED-5, 1958, 49.
- Runyan, W. R. Silicon Semiconductor Technology. New York: McGraw-Hill, 1965.
- Ryder, R. M. and Kircher, R. J. Bell Systems Technical Journal, 28, (1949), 370.
- Saby, J. S. Proceedings IRE, 40, (1952), 1358.
- Satoda, Y. and Bodway, G. E. IEEE Journal of Solid-State Circuits, SC-3 (1968), 250.
- Shockley, W. Bell Systems Technical Journal, 28 (1949), 435.
- Shockley, W., Sparks, M., and Teal, G. K. Physical Review, 83, 1951, 151.
- Sigler, J. and Watelski, S. B. Solid-State Journal, 2 (1961), 33.
- Sze, S. M. and Gibbons, G. Solid-State Electronics, 9, (1966), 831.
- Taylor, C. J. NASA Contractor Report. Report number NASA CR-597 to the National Aeronautics and Space Administration, 1966.
- Thomas, D. E. and Moll, J. E. Proceedings IRE, 46, (1958), 1177.
- Uzunoglu, V. and White, M. H. Semiconductor Products and Solid-State Technology, Feb. 1, 1965.
- Wallace, R. I., et al. Proceedings IRE, 40, (1952), 1395.
- Wang, P. Solid-State Technology, 12, (1969), 25.

Westinghouse Staff of Science and Technology. Integrated Electronic Systems. New York: Prentice-Hall, 1970.

Wheeler, H. A. IEEE Transactions on Microwave Theory and Techniques, MTT-12, (1964), 280.

Wheeler, H. A. IEEE Transactions on Microwave Theory and Techniques, MTT-13, (1965), 172.